Response to the Reviewer 1's Comments

Blue: Reviewer's comment,

Black: Response to the comment,

Red: Lines added or modified in the revised manuscript

While I think the general idea of the paper – to study how much lateral viscosity variations (LVV) due to temperature and strain rate dependence may help to explain the discrepancy between the (higher) amplitudes of dynamic topography inferred from mantle flow and the (lower) residual topography estimates based on observations is useful in that it addresses an unresolved problem, and I also appreciate the relatively simple setup, which should help with gaining a qualitative understanding, I think the current paper suffers from several shortcomings, which limit its usefulness.

Firstly, the parts without LVV add nothing new to what is already known. Of course, I realize that these are mainly meant for comparison with the later results with LVV. But that a contrast between low-viscosity mantle and high-viscosity lithosphere leads to increased dynamic topography, and the topography gets higher the stronger and/or thicker the lithosphere is, and that an asthenospheric low-viscosity channel leads to reduced topography can all be inferred from topography kernels (see e.g. my papers from 2001 doi:10.1016/S0012-821X(01)00229-1 Fig. 2 and 2016 doi:10.1093/gji/ggw040 Fig. 3), for a broad range of depths and size of anomalies (corresponding to spherical harmonic degree). In contrast, your results are just for particular anomaly depths and (rather small) size compared to what is seen in tomography.

We agree with the reviewer that the arguments at the beginning of the paper can be derived from radial stress or topography kernels for all wavelengths and depths (Hager and Clayton, 1989; Richards and Hager, 1989; Steinberger et al., 2001; Steinberger, 2016). As also pointed out by the reviewer, we imposed in our model a particular depth in the upper mantle and a relatively smaller anomaly size. It's true that one could follow a spherical harmonics approach in addressing dynamic topography. However, when the viscosity has lateral variations, spherical harmonic analysis becomes relatively hard to investigate analytically. When the mantle has non-linear rheology, all wavelengths of dynamic topography become coupled, and the degree of coupling should depend on how viscosity varies with temperature, pressure and strain-rate. Previous estimates using perturbation theory are insightful on understanding the impact of horizontal harmonic variations in viscosity on the dynamic topography as well the geoid (Richards and Hager, 1989), however these models assume that the lateral viscosity variations are *in phase* with the density anomalies, which is not necessarily the case in power-law rheology which introduces additional radial and lateral variations in viscosity as we show in our numerical models. Therefore, the variations in viscosity driven by a density anomaly in the upper mantle can reach well beyond the spatial dimensions of the embedded anomaly, and affects the mechanical lithospheric thickness. In that case, the dynamic topography varies considerably from the case where the mantle is isoviscous.

Based on above arguments, in our manuscript, we first introduced the Morgan (1965)'s analytical work on dynamic topography which uses radially layered viscosity model (up to two layers) for the Earth's interior. This helps us to easily compare it with more complex numerical models in the case for upper mantle density anomalies. Regarding the size of the anomaly, we explained our reasoning. A small radius minimizes the artefacts in the calculations and provides a better comparison with the analytical solutions carried out in an infinite half-space. The aim of this paper is not to predict the dynamic topography by using a density model derived from a seismic tomography (Steinberger et al., 2001, 2019; Flament et al., 2013), but to give insights on the first order changes in dynamic topography driven by non-linear rheology of the mantle. Having said that, we agree with the reviewer's point that the impact of larger anomalies, especially in the lower mantle, should be considered in future works.

I think for such small scales the effect of a low viscosity asthenosphere channel are stronger than for the larger scales seen by seismic tomography. E.g. in my 2016 paper Fig. 9a I find that one needs a very strong reduction in asthenosphere viscosity in order to get an appreciable reduction in topography, if anomalies are inferred from tomography. So I think the comparatively strong reductions in topography you show for a low-viscosity channel are partly misleading.

The assumptions about lithospheric thickness and radial viscosity may be effective in concluding the above mentioned argument. At the length-scales of our work (<1,000 km), the viscosity contrast as well reduction in the mechanical thickness of the lithosphere (via viscosity) affects the amplitude of dynamic topography. However, at longer scales (e.g. degree 2) with only radial variation in viscosity and imposed lithospheric thickness, one may need strong reduction in asthenospheric channel viscosity in order to get appreciably lesser amplitudes of dynamic topography. Furthermore, extra caution is necessary when comparing global seismic tomography models having horizontal resolutions of hundreds of km which is appreciably higher than the resolution of our numerical models (6-10 km's).

Also, in my Tectonophysics paper (doi:10.1016/j.tecto.2017.11.032) I find that the largest discrepancy by more than a factor 2 is at spherical harmonic degree two, whereas the discrepancy is much smaller at higher spherical harmonic degrees (i.e. smaller scales). It seems that your results could mainly explain a discrepancy at small scales, whereas the real discrepancy is at very large scales, and your results cannot explain this.

We agree that our model setup is not the best option to address the discrepancy at longest wavelengths or lowest harmonic degrees. We mentioned on the wavelengths being investigated in our numerical models by adding the following on Lines 20-22 in the revised text: "*Our experiments show that, at relatively short wavelengths (<1,000 km), the amplitude of dynamic topography, in the case of non-Newtonian mantle rheology, is reduced by a factor of ~2 compared to isoviscous rheology.*" However, we note that in non-Newtonian rheology, all wavelengths are coupled (Richards and Hager, 1989) and the dynamic topography at spherical harmonic degree 2, to a certain extent, will be influenced. In that regard, we added the following (on Lines 25-27 in the revised text): "*Although our results are strictly valid for flow wavelengths less than 1,000 km, we note that in non-Newtonian rheology all wavelengths are coupled, and the dynamic topography will be influenced.*" We would like to note that we seek to further investigate the effect of mantle viscosity on dynamic topography at longer wavelengths in the future.

Secondly, I think the usefulness of the models with LVV is severely limited because of the limitation of viscosities to the interval 10**19 Pas to 10**22 Pas. In this way, model 4b is almost the same as model 1 with constant viscosity (and giving very similar amplitude), model 4a approximately corresponds to the 2-layer model with topography accordingly increased, and model 5b has a low-viscosity channel with topography accordingly reduced. What I am puzzled about, though is that case 5a gives almost the same topography as 4a although it is also two-layer (although with thinner lithosphere). I think this limitation kind of beats the purpose of introducing a realistic rheology, because models essentially turn out to be a more complicated implementation of the easier models without LVV above. Also, I expect that without a cutoff, lowering activation enthalpy would not only lead to overall reducing viscosity, but also reducing viscosity contrasts. So, in contrast to your results I would expect a weaker lithosphere-asthenosphere contrast, and hence reduced dynamic topography for the lower activation enthalpy.

Exp. 5a and Exp 4a gives not similar topographies although their viscosity fields look like two-layer and similar to each other. As the reviewer pointed, the thickness of the lithosphere in both experiments are different, as of Exp4a having higher lithospheric thickness and therefore larger amplitude of dynamic topography. In Figure 7a of the manuscript, we show that, in Exp. 5a, the thickness of the lithosphere (in terms of viscosity) is reduced by about 30 to 45 km in comparison to Experiment 4a, which delivered a dynamic topography of ~149 m (in Exp. 5a) with the same viscosity contrast (Figure 7b,c). This experiment confirms that different mantle rheology results in different lithospheric thickness through local changes in viscosity. This is one of the key ideas of this paper.

In response to the reviewer's comment on the viscosity window, we run models with higher viscosity range. We increased the permitted viscosity range by two order of magnitude from [10^{19} Pa·s - 10^{22} Pa·s] to [10^{18} Pa·s - 10^{23} Pa·s]. In order to have better accuracy in the calculations, we kept the penalty value for convergence of the solution as low as before (0.03), however, due to our limitation on the resolution, the solutions had second order variations that we had to further smooth out the topography curves before picking their peak values. In the following supplementary figure 1, we plot the ratio of the viscosity field in the supplementary models to the viscosity field of the models in the manuscript, for each rheology and activation energy, along the same 2D cross-section. We give the change in dynamic topography, in percentage, also the minimum and maximum variation in viscosity across the entire numerical model. We also plot the viscosity ratio profile at the centre of the model (Fig. S2). In all rheologies, the lithosphere tends to have higher viscosity, if allowed, and the asthenosphere viscosity between the anomaly and the base of mechanical lithosphere doesn't show increase as much as the lithosphere. This results in an overall increase in viscosity contrast, therefore promotes an increase in dynamic topography. However, the magnitude of such increase was not notable because viscosity variations also affect the lithospheric mechanical thickness and/or the thickness of the low viscosity asthenospheric channel, which play a role in determining the amplitude of dynamic topography. In the case with dry olivine with low activation energy (Fig. S1-a), the viscosities inside the density anomaly show decrease, but the viscosities in the lithosphere show an overall increase. This results in a gradual increase in viscosity contrast between the lithosphere and asthenosphere, but also with modulation of the topography by the lower crust, limiting the increase in dynamic topography to 7.5 m. With dry olivine rheology with higher activation energy (Fig. S1-b) results in an increase in viscosity nearly across the entire cross-section, giving gradual increase in viscosity contrast between the mechanical lithosphere and asthenosphere above the anomaly. However, the thickness of the low viscosity asthenospheric channel is also increased, which is dominating the dynamic topography and resulting in gradual decrease by about 5 metres. The response of the dynamic topography to varying rheologies is similar in wet olivine rheology. These indicate that the viscosity window we used in the models doesn't severely limit the usefulness of them. However, we mentioned this variation (~5%) in the revised version of the manuscript by adding the following on Lines 329-333 in the revised text: "*Using a larger viscosity range in the models ($10^{18} Pa \cdot s \leq \eta(P,T,\dot{\varepsilon}) \leq 10^{23}\ Pa \cdot s$) resulted in ~5% variation in the amplitude of dynamic topography, indicating that the effects of non-linear rheology are reasonably captured in our models with smaller viscosity range ($10^{19} Pa \cdot s \leq \eta(P,T,\dot{\varepsilon}) \leq 10^{22}\ Pa \cdot s$).*"

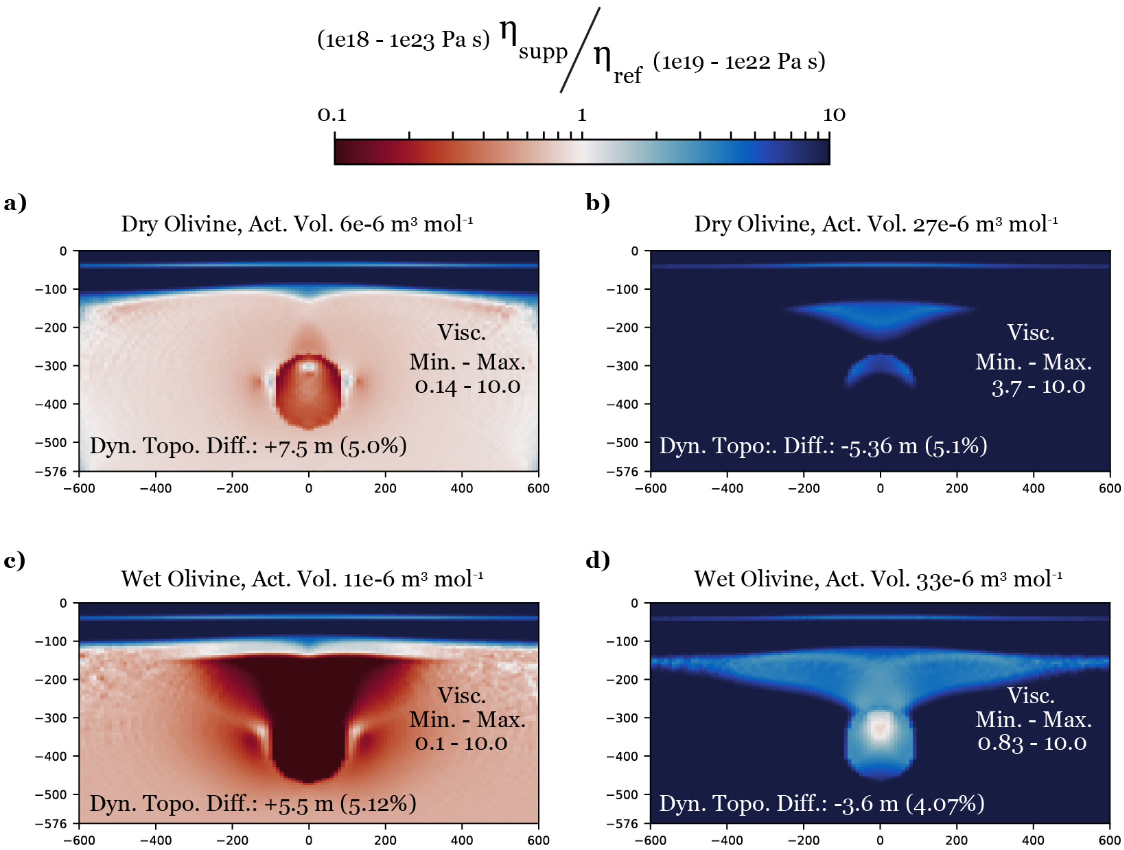

Figure S1: The ratio of viscosity fields of the supplementary models having wider viscosity window of 10^{18} Pa·s to 10^{23} Pa·s, to the models in the manuscript using a relatively narrower viscosity window of 10^{19} Pa·s to 10^{22} Pa·s. The change in dynamic topography and variation in min. and max. viscosities are given in the lower-left and middle-right for each model.

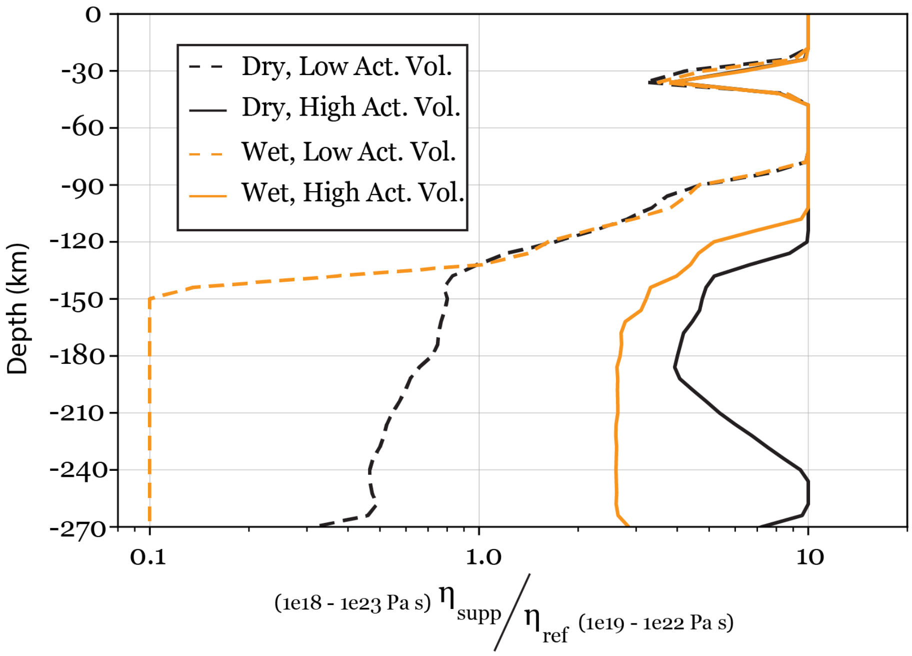

Figure S2: Variation of viscosities (ratios) at the centre of the numerical models.

Furthermore, reduction in activation enthalpy does result in overall reduction in viscosity, but the viscosity function also depends non-linearly on the strain rate, which strongly modulates this reduction, and introduces viscosity contrasts between different regions in the upper mantle. However, this effect could be lessened in diffusion creep.

In the following are a few more consecutive comments: l.54: as said, this large discrepancy is at the very largest scales, much larger than your model.

Thanks, we modified that line of the text accordingly by replacing the line stating: "*The problem is that dynamic topography predictions derived from mantle convection models are generally larger by a factor of two than estimates from residual topography (Cowie and Kusznir, 2018; Flament et al., 2013).*" with the following in the revised text (Lines 55-58) *"The problem is that dynamic topography predictions derived from mantle convection models are generally larger by a factor of two (more significant at the very large scales) than estimates from residual topography*

(Hoggard et al., 2016; Cowie and Kusznir, 2018; Davies et al., 2019; Steinberger et al., 2019)."

l. 220 this equation could actually be quite simplified. Because grain-size exponent p=0 the factor d**(p/n) is equal to 1 and therefore disappears. In each case, A**(-1/n)*f_H2O**(-r/n) is just a given number so you could simplify the equation in this way.

Thanks, we simplified that equation in Line 229 in the revised text. We kept other terms as it is because we use both dry and wet rheologies and different power-law exponent (crust vs. mantle).

l. 223 should be "volume and energy" (i.g. the other way round)

Thanks for the correction. We modified that sentence accordingly (Line 231 in the revised text).

l. 273 should be "wet olivine" (remove "dry").

Thanks for the correction. We modified it (Line 292 in the revised text).

l. 321 I don't know where I would have said in that paper that the misfit demands a scaling factor ~0.35, It it true that one needs to downscale shallow seismic anomalies, but I believe this has nothing to do with viscosity structure; it is rather because the thermal anomalies and corresponding seismic anomalies in the lithosphere are largely compensated by chemical anomalies, with a much smaller seismic signature.

We should have cited only (Cowie and Kusznir, 2018) because this argument is only made there. We corrected that sentence accordingly in the Lines 336-339 in the revised manuscript. We find the reviewer's point about chemical anomalies and viscosity structure at shallow depths speculative to a certain extent. Our numerical model do show that viscosity variations at shallow depths determine the effective lithospheric thickness which can strongly affect the amplitude of dynamic topography.

Fig 1 a: Why the results for Morgan Hard Sphere and Molnar Hard Sphere are different? I think they are both analytical results, so they should be identical.

Thanks for the question. It mainly results from the higher order term that Molnar et al. (2015) takes into account which is not considered in Morgan (1965). The term of interest is $\varepsilon^2 = \frac{a^2}{D^2}$ where a is the radius of the spherical density anomaly and D is the depth of the centre of the anomaly that is mentioned in Appendix A3 in Molnar et al. (2015). We briefly mentioned on this in Lines 95-98 in the revised manuscript. Now it reads as "*For the same problem, Molnar et al., (2015) provided a solution by considering a higher order term resulting in a slight difference with Morgan (1965a)'s solution (see Appendix A3 in Molnar et al. (2015)) allowing to consider density anomalies of finite viscosity (η_{sphere}) (Eq. 3)*".

Fig. 7c: Viscosity 10**20 Pas or 10**21 Pas at the lithosphere-asthenosphere boundary both seems much too low to me.

We inferred the lithosphere-asthenosphere *transition zone* from the numerical models. We understand that using lithosphere-asthenosphere *boundary* could be misleading because of the viscosities cited, however, it's also true that defining a lithosphere-asthenosphere *boundary* is helpful and necessary when comparing lithospheric thickness between different numerical models. Fig. 7a shows that the viscosities show strong decrease from 10^{22} Pa·s to 10^{19} Pa·s in a few tens of km, which is a typical lithosphere-asthenosphere transition profile with an exponential decay constant of 5-12 km (Conrad and Molnar, 1997). However, it's also possible that with the higher viscosity window, this transition zone could include higher viscosities as the reviewer would expect. We mentioned on this by adding the following in Lines 276-278: "*We infer the mechanical thickness of the lithosphere from the viscosity profiles plotted in Figure 7a, along which the lithosphere-asthenosphere transition zone shows a rapid decrease in viscosity (Conrad and Molnar, 1997).*"

Table 1: For better comparison with text and eq. 5, you could also include the symbols (in those cases where you have defined them) in another column. I think the units for the pre-exponential factor should be MPa**-ns**-n (not -1)

We added the symbols in another column in Table 1. We also mentioned on the brittle deformation law we had defined and density of rocks at depth in the numerical models, an information that was missing in the main text. We confirm that the units for the pre-exponential factor is $MPa^{-n}\ s^{-1}$.

l. 28: write "from the surface"

Thanks, we modified that sentence (Line 31 in the revised manuscript).

l. 65: better "dependence ... on" ?

Yes, that sounded much better. We modified the text accordingly (Lines 67-68 in the revised text).

References

Conrad, C. P. and Molnar, P.: The growth of Rayleigh-Taylor-type instabilities in the lithosphere for various rheological and density structures, , 95–112, 1997.

Cowie, L. and Kusznir, N.: Renormalisation of global mantle dynamic topography predictions using residual topography measurements for “normal” oceanic crust, Earth Planet. Sci. Lett., 499, 145–156, doi:10.1016/j.epsl.2018.07.018, 2018.
Davies, D. R., Valentine, A. P., Kramer, S. C., Rawlinson, N., Hoggard, M. J., Eakin, C. M. and Wilson, C. R.: Earth’s multi-scale topographic response to global mantle flow, Nat. Geosci., 12, 845–850, 2019.
Flament, N., Gurnis, M. and Müller, R. D.: A review of observations and models of dynamic topography, Lithosphere, 5(2), 189–210, doi:10.1130/L245.1, 2013.
Hager, B. H. and Clayton, R. W.: Constraints on the structure of mantle convection using seismic observations, flow models, and the geoid, 1989.
Hoggard, M. J., White, N. and Al-Attar, D.: Global dynamic topography observations reveal limited influence of large-scale mantle flow, Nat. Geosci., 9(6), 456–463, doi:10.1038/ngeo2709, 2016.
Molnar, P., England, P. C. and Jones, C. H.: Mantle dynamics, isostasy, and the support of high terrain, J. Geophys. Res. Solid Earth, 1–26, doi:10.1002/2014JB011724, 2015.
Morgan, W. J.: Gravity anomalies and convection currents: 1. A sphere and cylinder sinking beneath the surface of a viscous fluid, J. Geophys. Res., 70(24), 6175–6187, 1965.
Richards, M. A. and Hager, B. H.: Effects of lateral viscosity variations on long-wavelength geoid anomalies and topography, J. Geophys. Res. Solid Earth, 94(B8), 10299–10313, 1989.
Steinberger, B.: Topography caused by mantle density variations: observation-based estimates and models derived from tomography and lithosphere thickness, Geophys. Suppl. to Mon. Not. R. Astron. Soc., 205(1), 604–621, 2016.
Steinberger, B., Schmeling, H. and Marquart, G.: Large-scale lithospheric stress field and topography induced by global mantle circulation, Earth Planet. Sci. Lett., 186(1), 75–91, doi:10.1016/S0012-821X(01)00229-1, 2001.
Steinberger, B., Conrad, C. P., Osei Tutu, A. and Hoggard, M. J.: On the amplitude of dynamic topography at spherical harmonic degree two, Tectonophysics, 760(November 2017), 221–228, doi:10.1016/j.tecto.2017.11.032, 2019.

Response to the Reviewer 2's comments

Blue: Reviewer's comment,

Black: Response to the comment,

Red: Lines added or modified in the revised manuscript

The authors have performed numerical simulations of Stokes flow for a density anomaly in the mantle under a variety of different rheological assumptions. These simulations are benchmarked against analytical solutions for some of the simpler model setups. More complex behaviours are then explored, including using a power law rheology for which analytical solutions do not exist. The authors show that the rheological choices can have a profound impact on the observed dynamic topography observed at the surface.

The paper is mostly well written and contains a simple yet powerful illustration of some of the potential pitfalls in modelling dynamic topography. Some of the effects that are highlighted are already relatively well known, but are worth repeating and are useful in combination with the new results for the power-law rheology. My principal issue surrounds the motivation for the study, which is ostensibly concerning the amplitude mismatch between observed and predicted dynamic topography at long wavelengths (spherical harmonic degree ~ 2). However, I think that the model set up means that the main conclusions are probably more applicable for shorter wavelength features, and the significance for long-wavelengths mismatch remains under-explored. Nevertheless, I still think that this is an elegant illustration of some of the caveats associated with mantle convection modelling, and recommend that it be published in Solid Earth Discussions.

Main comment:

Discrepancy between observed and predicted dynamic topography: As you explain in Lines 41–55 there is a mismatch between the amplitude of observed residual topography and dynamic topography predicted from simulations. Over the last few years, there has been a general focus on the long-wavelength (degree 2) components, where the driving density anomalies have comparable lateral scales to the depth of the mantle. Instantaneous flow kernels (with no lateral viscosity variations) show that the effect of features such as a low viscosity asthenosphere are less pronounced at the lower degrees than at higher degrees (shorter wavelengths). Thus, I think that the experimental set up that you are using is more suited to comparison with shorter wavelength density anomalies, and the results on long-wavelength dynamic topography predictions could turn out to be less dramatic.

Nevertheless, I think that there is also potentially an issue with amplitudes at short wavelengths. Studies that attempt to include the shallow mantle tend to predict larger dynamic topography than we observe in residual topography (e.g. Steinberger, 2016; Steinberger et al., 2019; Davies et al., 2019). My suspicion is that the conversion between seismic velocity and density structure is largely to blame, but your results show that the rheological assumptions may also be a significant factor. I therefore think that the motivation in your study should probably be more nuanced than it is currently written.

We are thankful to the reviewer for insightful comments and we agree with the reviewer on points made about wavelength of the dynamic topography. In the revised version of our manuscript, we put more emphasis on the fact that, shorter wavelengths of dynamic topography are being explored and long-wavelengths are currently under-explored. We also mentioned that all wavelengths become coupled in a non-

Newtonian mantle (Richards and Hager, 1989) and a more realistic rheology for the upper mantle should be considered in future works.

We realize that our paper is well-timed with a recent work by Davies and colleagues presenting that it's of critical importance to consider the non-linear viscosity structure of the lithosphere and shallow upper mantle (i.e. dependence on pressure and temperature) on global mantle convection models to accurately predict Earth's dynamic topography (Davies et al., 2019). It's worth to mention that, in our models, the viscosity also depends on strain rate, which is critical in inducing local reductions in viscosity in regions far beyond the boundaries of the embedded density anomaly (i.e. at lower part of the lithosphere). This modulates the effective mechanical thickness of the lithosphere and affects the prediction for amplitude of dynamic topography.

We also find the reviewer's comment on the conversion between seismic velocity and density interesting, and useful to mention. We briefly added a statement about it to emphasize that such uncertainty might be playing a role in predicting the amplitude of dynamic topography in global mantle convection models (Lines 53-55 in the revised manuscript). However, in the revised manuscript, we decided not to expand further on this as that would be an undertaking beyond the scope of our paper.

Additional comments:

L15–17 (in abstract): In this sentence, it is unclear that you have shown that using a power law rheology reduces dynamic topography and so potentially helps to explain this discrepancy. Please clarify, particularly the final sub-clause.

Thanks. We clarified that sentence. Now, that part of the abstract reads as "*In this paper, we use 3D numerical experiments to evaluate the extent to which the dynamic topography depends on mantle rheology. We calculate the amplitude of* *instantaneous dynamic topography induced by the motion of a small spherical density anomaly (~100 km radius) embedded into the mantle. Our experiments show that, at relatively short wavelengths (<1,000 km), the amplitude of dynamic topography, in the case of non-Newtonian mantle rheology, is reduced by a factor of ~2 compared to isoviscous rheology.*"

L34: "...created by plate tectonic processes." I think this should be expanded further to improve clarity. Essentially, it is dominated by isostatic topography associated with variations in the thickness and density of sediments, crust and lithospheric mantle.

Thanks, we replaced this statement with the following (in Lines 36-38 in the revised manuscript): "*Because it is typically a low-amplitude and long-wavelength transient signal, it is often dwarfed by isostatic topography associated with variations in the thickness and density of sediments, crust and mantle lithosphere.*"

L34–39: I think that this section is a little misleading. There are two separate types of observation: i) the absolute amplitude of dynamic topography at the present-day and ii) the rate at which it is changing. Measurements of residual topography constrain the former, as you explain in the next paragraph. The couple of sentences here on sedimentary basins are more to do with the rates of change, and in that sense are a little out of context with the rest of the manuscript. I'd suggest either clarifying this issue or removing these sentences.

We agree with the reviewer. We removed those sentences that were out of the context with the rest of the text.

L43: "…isostatic components…" is a little vague. Specifically we want to remove isostatic topography arising from sediments, crustal structure and the lithospheric mantle if we want to investigate signals arising from deeper mantle convection.

We replaced "isostatic components" with "*isostatically compensated topography*" in Line 42 in the revised text.

L47: Rather than the accuracy of the measurements, it is more whether the measurements are truly a proxy for deeper mantle contributions that depends upon the factors you highlight here.

Thanks. We edited that sentence accordingly by removing "*the accuracy of…*". The new version is as follows (in Lines 46-48 in the revised manuscript): "*However, these residuals depend on our knowledge of the thermal and mechanical structure of the lithosphere, and therefore may not be an accurate estimation of the deeper mantle contribution to the Earth's topography.*"

L59: Repetition of "In this paper…".

Thanks, we deleted one of them.

L67: Replace "…lesser magnitude…" with "…lower amplitudes…".

Thanks, we edited that sentence.

L85: Replace ρ with $\Delta\rho$ and explain the difference between air and water-loaded dynamic topography.

Now, it reads as $\Delta\rho$ rather than ρ in the edited version, with a mention on the air and water-loaded case. The new version is as follows (in Line 89): "*where $\Delta\rho$ is the density difference between the mantle and air (or water assuming a sea-load when $e<0$)*

(Morgan, 1965a; Houseman and Hegarty, 1987). " We also simplified the equation a bit more (Eq. 2 in the revised text).

L95–96: This is a little hard to read and would benefit from clearer grammar.

Thanks, we simplified that sentence accordingly. We replaced "*...where* $C^2=D^2+x^2$ *and* $f = (\eta_1 + \frac{3\eta_{sphere}}{2})/(\eta_1 + \eta_{sphere})$*, for very viscous sphere* $(\eta_{sphere} \gg \eta_1)$ f*=1.5, and deformable sphere* $(\eta_{sphere} \cong \eta_1)$ f*<1.5.*" **with** "*...where* $C = \sqrt{D^2 + x^2}$ *and* $f = (\eta_1 + \frac{3\eta_{sphere}}{2})/(\eta_1 + \eta_{sphere})$*. One can find that f=1.5 if the sphere is very viscous* $(\eta_{sphere} \gg \eta_1)$*, and* $f < 1.5$ *for any other case.*"

L108: Replace \...normal total stress..." with \...total normal stress...".

Thanks, we reordered that collection of words in that line, and in places where we use them.

L109: \...mass anomaly per unit length..." - what length is this referring too?

Because Morgan (1965, p.6184) integrated a series of point mass sources spread continuously along a line, so that this term comes as a mass per unit length. We modified that sentence by giving more information in parenthesis (Lines 112-116 in the revised text): "*In this case, Morgan (1965a) showed (Eq. 4) that the total normal stress induced by the density anomaly is dependent on the mass anomaly per unit length* (M_u*, for point sources integrated along a continuous line), the depth of the centre of the sphere (D), and marginally on the ratio of the viscosity of the convective mantle to the viscosity of the lithosphere* ($R=\eta_1/\eta_2$)."

L111: This needs a lead in sentence. Something like \Total normal stress can be calculated in the Fourier domain according to..."

We put a beginning statement to indicate that this solution is derived in Fourier domain. The following is added (Lines 116-117 in the revised text): "*The 2-layer problem is treated in Fourier domain with the resulting total normal stress as below:*"

L122: Start this sentence with a clause like \Although unrealistic for the Earth, under the assumption where..."

Thanks, we added the following at the beginning of the mentioned sentence (Line 129): "*Although an unrealistic proposition for the Earth, …*"

L140: What is the purpose of this crustal layer? Is it an elastic lid? Does it have a rheology that deforms during the simulations? Please clarify. It does not show up in the Figure pictures.

This crustal layer exists in all models. It is visco-plastic, as the mantle, but with different viscous rheology (quartzite). The simulations were run to solve for instantaneous flow only; therefore, the defined crustal thickness (i.e. 42 km) is the same for all models. The crustal layer has been shown in Figure 2 and its physical properties were detailed in Table 1.

L159-160: Does this effect happen in all of your simulations?

We only tested the change in the sensitivity of the solution to the model geometry in a model with isoviscous rheology so that we could compare the resulting dynamic topography with the analytical solution in order to assess the boundary effects in the models. However, this effect could be slightly different for non-linear viscosities which we didn't pursue to investigate.

L169: Qualify what the asthenosphere here refers to. Is it the whole of the rest of your model domain beneath the lithosphere? How is the asthenosphere defined?

We clarified what we mean by asthenosphere, and lithosphere-asthenosphere boundary, as well as Figure 3. We prescribe a thermal gradient and the *thermal* lithosphere-asthenosphere boundary is defined by 1350 °C. We use the same thermal profile for all models, but for models using non-linear viscosity, the viscosity profile changes, so as the mechanical thickness of the lithosphere and thickness of asthenosphere. We added the following (Lines 274-278 in the revised text): "*We note that the viscosity contrast is attained by smoother transition between the lithosphere and asthenosphere (Fig. 7a, black dashed line). We infer the mechanical thickness of the lithosphere from the viscosity profiles plotted in Figure 7a, along which the lithosphere-asthenosphere transition zone shows a rapid decrease in viscosity (Conrad and Molnar, 1997).*"

L197-199: Good! This is a very clear and useful explanation of the cause of this behaviour.

Thanks. We are glad to know that our explanation of the decrease in amplitude of dynamic topography due to low-viscosity channel is useful to the readers.

L225-227: I did not know that this was generally accepted. Is this an opinion of the authors? Some back up references would be helpful. I agree that larger deviatoric stresses are thought to promote deformation by dislocation creep.

It is indeed generally accepted that in the convective mantle, low deviatoric stresses are not conducive to the activation of dislocation creep, and therefore that diffusion creep is the dominant strain mechanism (Karato and Wu, 1993, Turcotte and Schubert, 2002). In the vicinity of density anomaly, the deviatoric stresses are high enough for dislocation creep to dominate over diffusion creep. We supported our argument with references in Lines 233-236.

L169: Typo - currently reads \...creep of wet dry olivine..."

Thanks for picking this out. This was in Line 273, and we corrected it in the revised version of the manuscript (Line 292).

Figure 1: I think the y-axis in panel (b) would be better as dynamic topography for comparison to panel (a). Also, the key in (b) is a bit messy... A legend as in panel (a) would be clearer.

We modified Figure 1 and its caption based on the reviewer's suggestions.

Figure 3: These are great, but could do with standardising to make it a truly iconic figure. Could you i) add a line above the surface showing the dynamic topography (or state the peak value), ii) make all streamlines the same colour (either white or black), iii) place the key entries in their true depth order (lith, channel, asthen). I also think it could be clearer that the relative viscosity jumps between layers are what is important, rather than absolute values, but it is fine as is.

Thanks very much for the suggestions. We modified Figure 3 accordingly. The old and new versions are given below on the left and right columns, respectively.

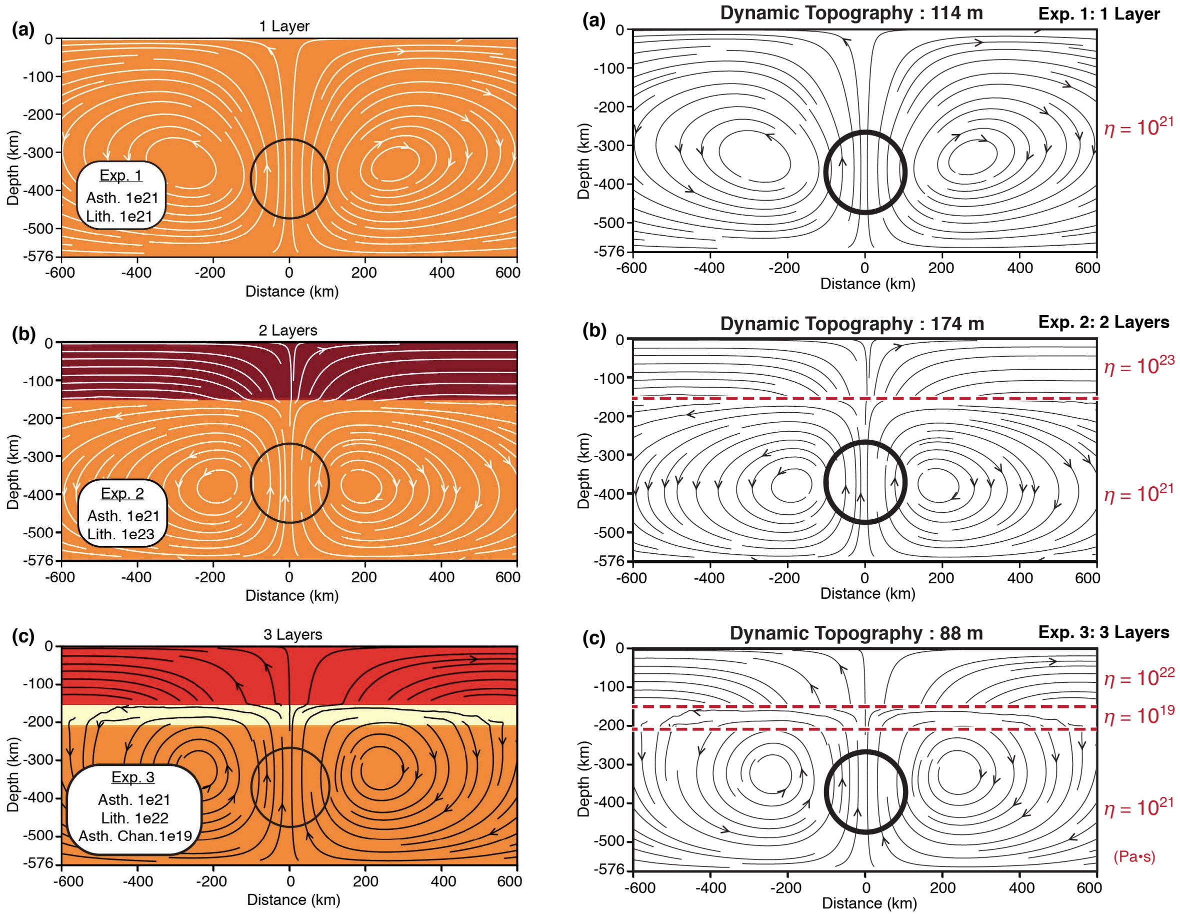

References

Davies, D. R., Valentine, A. P., Kramer, S. C., Rawlinson, N., Hoggard, M. J., Eakin, C. M. and Wilson, C. R.: Earth's multi-scale topographic response to global mantle flow, Nat. Geosci., 12, 845–850, 2019.

Houseman, G. A. and Hegarty, K. A.: Did rifting on Australia's Southern Margin result from tectonic uplift?, Tectonics, 6(4), 515–527, doi:10.1029/TC006i004p00515, 1987.

Karato, S. and Wu, P.: Rheology of the upper mantle: a synthesis., Science, 260(5109), 771–778, doi:10.1126/science.260.5109.771, 1993.

Morgan, W. J.: Gravity anomalies and convection currents: 1. A sphere and cylinder sinking beneath the surface of a viscous fluid, J. Geophys. Res., 70(24), 6175–6187, 1965.

Richards, M. A. and Hager, B. H.: Effects of lateral viscosity variations on long-wavelength geoid anomalies and topography, J. Geophys. Res. Solid Earth, 94(B8), 10299–10313, 1989.

The Impact of Rheological Uncertainty on Dynamic Topography Predictions

Deleted: : Gearing up for dynamic topography models consistent with observations

Ömer F. Bodur, Patrice F. Rey

EarthByte Group and Basin Genesis Hub, School of Geosciences, The University of Sydney, NSW 2006, Australia,

Correspondence to: Ömer F. Bodur (omer.bodur@sydney.edu.au)

Abstract

Much effort is being made to extract the dynamic components of the Earth's topography driven by density heterogeneities in the mantle. Seismically mapped density anomalies have been used as an input into mantle convection models to predict the present-day mantle flow and stresses applied on the Earth's surface, resulting in dynamic topography. However, mantle convection models give dynamic topography amplitudes generally larger by a factor of ~2, depending on the flow wavelength, compared to dynamic topography amplitudes obtained by removing the isostatically compensated topography from the Earth's topography. In this paper, we use 3D numerical experiments to evaluate the extent to which the dynamic topography depends on mantle rheology. We calculate the amplitude of instantaneous dynamic topography induced by the motion of a small spherical density anomaly (~100 km radius) embedded into the mantle. Our experiments show that, at relatively short wavelengths (<1,000 km), the amplitude of dynamic topography, in the case of non-Newtonian mantle rheology, is reduced by a factor of ~2 compared to isoviscous rheology. This is explained by the formation of a low viscosity channel beneath the lithosphere and a decrease in thickness of the mechanical lithosphere due to induced local reduction in viscosity. The latter is often neglected in global mantle convection models. Although our results are strictly valid for flow wavelengths less than 1,000 km, we

Deleted: has been given on extracting
Deleted: component
Deleted: , which is
Deleted: topographies
Deleted: topographies estimated from residual
Deleted: after extraction of
Deleted: . Our
Deleted: thermo-mechanical
Deleted: suggest that this discrepancy can be explained by the use of a viscosity model,
Deleted: doesn't account for non-linear viscosity behaviour. In this paper, we numerically model
Deleted: a
Deleted: When we use non-linear viscosities, our numerical models predict dynamic topographies lesser
Deleted: than those derived from numerical models using
Deleted: reduction in dynamic topography is
Deleted: either
Deleted: , or
Deleted: Furthermore, we show that uncertainties related to activation volume and fluid activity lead to variations in

note that in non-Newtonian rheology all wavelengths are coupled, and the dynamic topography at long wavelengths will be influenced.

Deleted: of about 20%.

1. Introduction

The Earth's mantle is continuously stirred by hot upwellings from the core-mantle boundary, and by subduction of colder plates from the surface into the deep mantle (Pekeris, 1935; Isacks et al., 1968; Molnar and Tapponnier, 1975; Stern, 2002). This introduces temperature and density anomalies that stimulate mantle flow and forces dynamic uplift or subsidence at the plates' surface (Gurnis et al., 2000; Braun, 2010; Moucha and Forte, 2011; Flament et al., 2013). Dynamic topography can affect the entire planet's surface with varying magnitudes. Because it is typically a low-amplitude and long-wavelength transient signal, it is often dwarfed by isostatic topography associated with variations in the thickness and density of sediments, crust and mantle lithosphere.

Deleted: topography created by plate tectonic processes. Therefore, investigations on dynamic topography signals mostly focus on non-tectonic regions where the dynamic topography can be extracted from the subsidence history of sedimentary basins. Dynamic subsidence and uplift events are identified by isolating part of the subsidence that cannot be explained either by thermal relaxation or tectonic processes such as crustal thinning .

For the present day, the observational constraints on dynamic topography come from residual topography measurements (Hoggard et al., 2016). Residual topography is calculated by removing the isostatically compensated topography from the Earth's topography (Crough, 1983; Cazenave et al., 1989; Davies and Pribac, 1993; Steinberger, 2007, 2016). Hoggard et al (2016)'s comprehensive work revealed that residual topography varies between ±500 m at very long-wavelengths (i.e. ~10,000 km) and can increase up to ±1,000 m at shorter wavelengths (i.e. ~1,000 km). However, these residuals depend on our knowledge of the thermal and mechanical structure of the lithosphere, and therefore may not be an accurate estimation of the deeper mantle contribution to the Earth's topography. Another approach to constrain present day Earth's dynamic topography involves numerical modelling of present-day mantle flow using seismically mapped density anomalies as an input (Steinberger, 2007;

Deleted: isostatic components

Deleted: .,

Deleted: the accuracy of

Deleted: estimates depends

Moucha et al., 2008; Conrad and Husson, 2009). However, this method requires a detailed knowledge of the viscosity structure in the Earth's interior (Parsons and Daly, 1983; Hager, 1984; Hager et al., 1985; Hager and Clayton, 1989), and translating seismic velocities to physical properties (e.g. temperature) of the mantle introduces further uncertainties (Cammarano et al., 2003). The problem is that dynamic topography predictions derived from mantle convection models are generally larger by a factor of two (more significant at the very large scales) than estimates from residual topography (Hoggard et al., 2016; Cowie and Kusznir, 2018; Davies et al., 2019; Steinberger et al., 2019). We hypothesise that this could be related to an oversimplification of the mantle rheology. In this paper, we explore how, at wavelengths less than <1,000 km, the magnitude of dynamic topography changes when we use a rheological model in which the viscosity depends on strain rate, temperature, pressure and fluid content. We first summarize the well-established analytical solution for calculating dynamic topography induced by a spherical density anomaly embedded into an isoviscous fluid (Morgan, 1965a; Molnar et al., 2015). Then, assuming isoviscous rheology, we illustrate that the amplitude of dynamic topography depends on the viscosity structure of the Earth's interior as shown by Morgan (1965a) and Molnar et al. (2015). Finally, we use 3D coupled thermo-mechanical numerical experiments of the Stokes' flow to assess the dependence of dynamic topography on nonlinear rheology using viscosity which depends on temperature, pressure, strain rate and fluid content. We show that plausible non-linear rheologies can induce local variations in viscosity and result in dynamic topography of lower amplitude compared to those derived from models using isoviscous rheology.

2. Dynamic topography driven by a rising sphere: Analytical and numerical solutions

2.1 Analytical solution for one layer isoviscous fluid

Deleted: good

Deleted: .

Deleted: viscous behaviour of the flowing

Deleted: is impacted

Deleted: viscosity

Deleted: In this paper,

Deleted: .

Deleted: 3-D

Deleted: dependency

Deleted: to

Deleted: more realistic rheology

Deleted: lesser magnitude of

Deleted: than

We assume here a simple 2D model representing a very viscous spherical density anomaly embedded into a semi-infinite isoviscous fluid bounded by an upper free surface. Earliest analytical investigations revealed that, albeit counter-intuitive, the magnitude of the induced surface deflection due to the rising sphere is independent of the viscosity of the fluid. The dynamic topography is a function of the vertical total stress (σ_{zz}) applied to the surface which is proportional to the size and depth of the density anomaly according to Equation 1 (Morgan, 1965a, 1965b).

$$\sigma_{zz}(x,0) = [2g\delta\rho r^3]\frac{D^3}{(D^2+x^2)^{5/2}} \quad (1),$$

where g is the gravitational acceleration, $\delta\rho$ is density difference between the anomaly and the ambient material, r is radius of the sphere, and D is distance from the surface to the centre of the anomaly (modified from Morgan 1965a, see Figure 1a). The dynamic topography e is given by:

$$e(x) = \frac{\sigma_{zz}(x,0)}{g\,\Delta\rho} \text{ at } z = 0 \quad (2),$$

where $\Delta\rho$ is the density difference between the mantle and air (or water assuming a sea-load when e<0) (Morgan, 1965a; Houseman and Hegarty, 1987). In Figure 1a, we plot the dynamic topography induced by a sphere of 1% density anomaly, whose centre is at 372 km depth (D= 372 km) below the free surface. We calculate the vertical total stress and convert it to dynamic topography by using Equation 2 for different values of the radius of the sphere. The amplitude of dynamic topography shows an accelerating increase by cubic dependence on the radius of the spherical density anomaly (Fig. 1a, black solid line). For the same problem, Molnar et al., (2015) provided a solution by considering a higher order term resulting in a slight difference with Morgan (1965a)'s solution (see Appendix A3 in Molnar et al. (2015)) allowing to consider density anomalies of finite viscosity (η_{sphere}) (Eq. 3):

$$\sigma_{zz}(C,0) = \frac{-\delta\rho r^3 D}{3f}\left[\frac{3-2f}{C^3} + \frac{18(f-1)r^2}{C^5} + \frac{6fD^2}{C^5} - \frac{30(f-1)r^2D^2}{C^7}\right] \quad (3),$$

Deleted: e_{zz}

Deleted: $e_{zz}(x,0)$

Deleted: $\frac{\sigma_{zz}(x,0)}{\rho g}$

Deleted: ρ

Deleted: density

Deleted: Eqn

where $C = \sqrt{D^2 + x^2}$ and $f = (\eta_1 + \frac{3\eta_{sphere}}{2})/(\eta_1 + \eta_{sphere})$. One can find that f=1.5 if the sphere is very viscous ($\eta_{sphere} \gg \eta_1$), and f< 1.5 for any other case. In Figure 1a, we present two more plots of dynamic topography where f = 1.5 for hard sphere and f = 1.25 for $\eta_{sphere} = \eta_1$ by using Equation 2 and 3. Figure 1a shows that a rising deformable sphere creates higher dynamic topography compared to a very viscous sphere. These show that the viscosity contrast between the spherical anomaly and the surrounding material can affect the dynamic topography. In the section that follows, we explore how dynamic topography varies when there is layering in viscosity, such as presence of a strong lithosphere above the convective mantle.

2.2 The impact of layered viscosity structure on dynamic topography

A more generalized solution has been put forward to accommodate the presence of a stronger upper layer representing a lithosphere with viscosity η_2 above a weaker layer with viscosity η_1 and with $\eta_1 < \eta_2$ representing the convective mantle (Fig. 1b). In this case, Morgan (1965a) showed (Eq. 4) that the total normal stress induced by the density anomaly is dependent on the mass anomaly per unit length (M_u for point sources integrated along a continuous line), the depth of the centre of the sphere (D), and marginally on the ratio of the viscosity of the convective mantle to the viscosity of the lithosphere ($R=\eta_1/\eta_2$). The 2-layer problem is treated in Fourier domain with the resulting total normal stress as below:

$$\sigma_{zz}(x,0) = \int_0^\infty \sigma_n \cos nx \; dn \quad (4),$$

where

$$\sigma_n = \frac{M_u g e^{-n(D-d)}}{2\pi(RS_h + C_h)} \left\{1 + n(D-d) + nd\left[\frac{1 - nD + n(D-d)(RC_h + S_h)/(RS_h + C_h)}{1 + nd(1-R^2)/(RS_h + C_h)(RS_h + S_h)}\right]\right\}$$

and C_h=*cosh nd*, and S_h=*sinh nd* (n is the wave number) and d is the upper layer thickness (modified from Morgan 1965a). Following Morgan (1965a), Figure 1b illustrates the relative importance of R as well as the ratio of the thickness of the upper layer to the depth of the

Deleted: $C^2=D^2+x^2$
Deleted:), for
Deleted: sphere
Deleted:) f=1.5,
Deleted: deformable sphere ($\eta_{sphere} \cong \eta_1$)
Deleted: <
Deleted: .
Deleted: give
Deleted: =
Deleted: existence
Deleted: anomaly
Deleted: the
Deleted: (η
Deleted:)
Deleted: lower
Deleted: (η_1, with $\eta_1 < \eta_2$ in
Deleted: Eqn
Deleted: total
Deleted: at depth
Deleted:), its depth

anomaly (d/D). As long as the lithosphere is more viscous than the asthenosphere, the vertical total stress at the surface has a minor dependence on the viscosity of the lithosphere (see solid lines with R=1 and R=0.01 in Fig. 1b). Figure 1b also shows that the magnitude of dynamic topography increases as the density anomaly is brought closer to the surface (compare for R=1 the solid black line and the dashed black line). Moreover, its sensitivity on the relative viscosity of the lithosphere also increases. Although an unrealistic proposition for the Earth, when the lithosphere is less viscous than the asthenosphere, the normal stress is much reduced and is strongly dependent on the viscosity of the lithosphere (Fig. 1b). These demonstrate that layering in viscosity can have a strong impact on the amplitude of dynamic topography (Sembroni et al., 2017). In the next section, we use the analytical solutions above to benchmark a numerical model, which we will then extend to non-linear viscosity.

Deleted: with R=1

Deleted: with R=1

Deleted: Under the assumption where

2.3 Numerical solutions

For comparison with analytical solutions (Morgan, 1965a; Molnar et al., 2015), we consider 3D numerical models involving 1, 2 and 3 isoviscous layers. These benchmark experiments will be used as references for non-isoviscous models discussed in section 3. We use the open-source code *Underworld* which solves the Stokes equation at insignificant Reynolds number (Moresi et al., 2003, 2007). The 3D computational grid represents a domain 3,840 km x 3,840 km x 576 km with a resolution of 6 km along the vertical z axis and 10 km along the x and y axes (Fig. 2). In all experiments, we include a 42 km thick continental crust above the upper mantle. The density structure is sensitive to the geotherm via a coefficient of thermal expansion and compressibility (see Table 1 for all parameters). The geotherm is defined using a radiogenic heat production in the crust, a constant temperature of 20ºC at the surface, and a constant temperature of 1,350ºC at 150 km. We disregard the adiabatic heating and the asthenosphere is kept at 1,350ºC. We embed a positive spherical temperature anomaly

Deleted: the

Deleted: Taking advantage of the symmetry of the experimental setup, we extract viscosity and velocity fields along a 2D cross section passing through the centre of the thermal anomaly, from which we get streamlines and vertical velocity profile along the vertical axis at the centre of the models. We calculate the dynamic topography from the normal stress computed at the surface.

Deleted: Stokes'

Deleted: value

Deleted: (see Table 1 for all parameters thermal parameters)

Deleted: .

Deleted: At a depth of 372 km below the surface, of +324ºC at a depth of 372 km below the surface, which delivers a 1% volumetric density difference. The radius of the sphere is 96 km. In all experiments, we impose free slip velocity boundary conditions at all walls, such as V_x and V_y are set to be free, but V_z = 0 cm yr^{-1} at the top wall. Taking advantage of the symmetry of the experimental setup, we extract viscosity and velocity fields along a 2D cross section passing through the centre of the thermal anomaly, from which we derive the streamlines and vertical velocity profiles along the vertical axis at the centre of the models. We calculate the instantaneous dynamic topography from the normal stress computed at the surface.

2.3.1 Dynamic topography due to a rising sphere in an isoviscous fluid

In the first experiment (Fig. 3a Experiment 1), we assign the same depth-independent viscosity of 10^{21} Pa s to the crust, mantle and the density anomaly. The streamlines for Experiment 1 (Fig. 3a) show formation of two convective cells at the sides of the sphere covering the entire crust and mantle. The vertical velocity profile indicates that the thermal anomaly rises with a peak velocity of ~2.4 cm yr^{-1}, which is faster than the 2.0 cm yr^{-1} predicted by the analytical solution (Fig. 4a). Experiment 1 predicts dynamic topography of 114 m (Fig 4b) which is lower than 132 m predicted by Molnar et al (2015)'s analytical solution. We have verified that increasing the depth of our model from 576 km to 864 km increases the dynamic topography from 114 m to 122 metres. Therefore, we attribute the misfit in amplitude of dynamic topography to the finite space in our numerical experiments. Our numerical experiment using isoviscous material delivers a result globally consistent with the analytical solutions of Morgan (1965a) and Molnar et al (2015).

Deleted: 0 cm yr^{-1} at the top wall.

Deleted: constant

Deleted: is rising

Deleted: a

Deleted: .,

Deleted: arises from

Deleted: compared to the semi-infinite half-space used in the analytical solution

Deleted: .,

2.3.2 Dynamic topography on a strong lithosphere above an isoviscous asthenosphere

In Experiment 2, we assign to the lithosphere a constant viscosity 100 times larger (10^{23} Pa s) than that of the asthenosphere (10^{21} Pa s, Fig. 3b) between z=150 km and base of the model. The convective cells become narrower by the induced viscosity contrast (Fig. 3b). The streamlines are deflected across the lithosphere-asthenosphere boundary due to the large viscosity contrast (Fig. 3b), and there is a sharp variation in vertical velocity at the base of the lithosphere (Fig. 4a, red solid line). The maximum vertical velocity ~2.1 cm yr^{-1} is attained near the centre of the anomaly. When compared to Experiment 1, the dynamic topography (Fig. 4b, red solid line) shows a significant increase from ~114 m to ~174 m. This increase is consistent with analytical estimations showing an increase in dynamic topography when viscosity increases toward the surface (Fig. 1b, R<1). In Experiment 2a (not shown here), we tested a different ratio of thickness of the lithosphere to the depth of the anomaly (see *d/D* in Equation 4) by increasing the lithospheric thickness from 150 km to 200 km, while keeping all parameters identical to those of Experiment 2. As predicted by Eq. 4, Exp. 2 predicted dynamic topography of ~191 m, being the largest among all experiments (Fig. 4b, red dashed line). Overall, and perhaps counter-intuitively, the presence of a thick viscous lithosphere enhances the dynamic topography. Interestingly, in analogue experiments where density anomaly is allowed to rise and interact with the lithosphere, the amplitude of the dynamic topography is inversely correlated with the thickness of the lithosphere (e.g. Griffiths et al. 1989; Sembroni et al. 2017).

2.3.3 The impact of low viscosity channel on the dynamic topography

Deleted: i.e.

Deleted: i.e.

Deleted:). This layering results in a decrease in thickness

Deleted: asthenosphere. As a result,

Deleted: are

Deleted: of

Deleted: for the case where

Deleted: see

Deleted: Eqn

Deleted: the model gives a

Deleted: highest

In Experiment 3 (Fig. 3c), we introduce a third 60 km thick low viscosity layer (i.e. 10^{19} Pa s) beneath the base of the lithosphere. The existence of a low viscosity layer has been discussed in several studies (e.g. Craig and McKenzie, 1986, Phipps Morgan et al. 1995, Stixrude and Lithgow-Bertelloni, 2005, and Becker, 2017). In this experiment, in order to prevent large viscosity contrast that can impede the numerical convergence, the viscosity of the lithosphere and that of the asthenosphere is set to 10^{22} Pa s and 10^{21} Pa s, respectively. When compared to Experiment 1, streamlines indicate a further decrease in size of the convective cells, and more importantly, a strong horizontal divergence of the streamlines within the low viscosity layer (Fig. 3c). The vertical velocities are also enhanced in the asthenosphere reaching up to ~2.8 cm yr^{-1} slightly above the centre of the anomaly (Fig. 4a, orange solid line). When compared to Experiment 1, we observe a strong reduction in dynamic topography (Fig. 4b, orange solid line) from 114 m to 88 m. This is due to the damping effect of the low viscosity channel that acts as a decoupling layer, which reduces the deviatoric stress through its ability to flow.

Until now, the viscosities were assumed to be constant. However, results from experimental deformation on mantle rocks strongly suggest that the viscosity is highly nonlinear (Hirth and Kohlstedt, 2003). In what follows, we explore the influence of more realistic viscosities on dynamic topography.

3. The impact of nonlinear viscosity on dynamic topography

3.1 Viscosity structure of the Earth's interior

Earth's mantle is not isoviscous. Geological records of relative sea level changes related to postglacial rebound, geophysical observations of density anomalies inferred from seismic velocity variations in the mantle and satellite measurements of the longest wavelength

Deleted: suggested by

Deleted: works

Deleted: ambient

Deleted: are

Deleted: as

Deleted: , and reach

Deleted: This low viscosity channel acts as a decoupling layer.

Deleted: aggregates

components of the Earth's geoid have been used to infer the radial viscosity profile of the Earth's interior (Hager et al., 1985; Forte and Mitrovica, 1996; Mitrovica and Forte, 1997; Kaufmann and Lambeck, 2000). Henceforward, beneath the lithosphere, a variation in viscosity up to two orders of magnitude has been proposed (e.g., Kaufmann and Lambeck, 2000). Investigations of the rheological properties of crustal and mantle rocks via rock deformation experiments revealed a nonlinear dependence of viscosity on applied deviatoric stress, pressure, temperature, grain size and the presence of fluids (Post and Griggs, 1973; Chopra and Paterson, 1984; Karato, 1992; Karato and Wu, 1993; Gleason and Tullis, 1995; Ranalli, 1995; Hirth and Kohlstedt, 2003; Korenaga and Karato, 2008). These experiments lead to the following relationship:

$$\eta_{eff}(\dot{\varepsilon}, P, T) = A^{\left(\frac{-1}{n}\right)} f_{H_2O}^{\left(\frac{-r}{n}\right)} \dot{\varepsilon}^{\left(\frac{1}{n}-1\right)} e^{\left(\frac{Q+PV}{nRT}\right)} \quad (5).$$

Deleted: $d^{\left(\frac{p}{n}\right)} f_{H_2O}^{\left(\frac{-r}{n}\right)}$

where $\dot{\varepsilon}$ and A stands for strain rate and pre-exponential factor; r and n are exponents for water fugacity (f_{H_2O}) and deviatoric stress, respectively; V and Q are the volume and energy of activation.

Deleted: σ,

Deleted: differential stress,

Deleted: *p*,

Deleted: grain size (*d*),

Deleted: and volume

In the case where mantle flow is driven by the temperature difference at the boundary of the convective layer or by internal heating, the dominant strain mechanism is diffusion creep because low deviatoric stresses are expected in the weak convective mantle (Karato and Wu, 1993; Turcotte and Schubert, 2002). However, mantle flow in the vicinity of a moving density anomaly is likely driven by deviatoric stresses that exceed the threshold for dislocation creep. In this case, nonlinear viscosities lead to strong local variation in viscosity. Are those local variations in viscosity important for dynamic topography? To answer this question, we need reasonable constraints on the rheological parameters controlling the viscosity of mantle rocks. However, the extrapolation from laboratory strain rates typically in the range of 10^{-6} s^{-1} to 10^{-4} s^{-1} to mantle conditions where strain rates are typically on the order of 10^{-13} s^{-1} results in significant uncertainties on the activation volume, activation energy and stress exponent (Hirth

Deleted: .

Deleted: in the vicinity of the moving density anomaly.

Deleted: rocks'

and Kohlstedt, 2003; Korenaga and Karato, 2008). In what follows, we explore how nonlinear viscosity impacts the dynamic topography and address how the uncertainties on the activation volume can affect dynamic topography.

In Experiments 4 and 5 (Fig. 5), the viscosity depends on temperature, pressure and strain rate as indicated by Equation 5, using published visco-plastic rheological parameters for the crust and mantle. Specifically, we use quartzite rheology for the crust (Ranalli, 1995), and test both dry and wet olivine rheologies for the mantle (Hirth and Kohlstedt, 2003). Other parameters are identical to those in Experiments 1-3. We give all the rheological and thermal parameters in Table 1. For a given olivine rheology (i.e. dry or wet) we vary the activation volume by using the minimum and maximum reported values (Hirth and Kohlstedt, 2003).

In the numerical models, the plastic (i.e. brittle) deformation is described via:

$$\tau = \mu\sigma_n + C_0 \quad (6)$$

where τ is the 2nd invariant of the deviatoric stress tensor, which varies with the coefficient of friction (μ), and depth via lithostatic pressure (σ_n), as well as the cohesion (C_0). Due to strain weakening, the cohesion and coefficient of friction decrease from C_0 = 10 MPa and μ_0 = 0.577 to C_0 = 2 MPa and μ_1 = 0.017 at which the maximum plastic strain (ϵ_{max}) is reached (i.e. 0.2, Table 1). The effective density (ρ) of rocks is determined by the pressure and temperature using the following equation:

$$\rho = \rho_0 [1- \alpha(T-T_0)] [1+ \beta(P-P_0)] \quad (7)$$

where ρ_0, T_0, α, and P_0 signify the reference density and temperature, thermal expansion coefficient, and the compressibility respectively.

3.2 Numerical results: the case of dry olivine

Deleted: the

Deleted: 5), we use published visco-plastic rheological parameters for the crust and mantle, therefore

Deleted: .

Deleted: upper

Deleted: particular

In Experiments 4a and 4b, we consider dry dislocation creep for olivine ($n > 1$, $p = 0$, $r = 0$). The reported activation volume for this rheology varies between 6x10^{-6} m^3 mol^{-1} and 27x10^{-6} m^3 mol^{-1} (Hirth and Kohlstedt, 2003). In Experiment 4a (Fig. 4b), we test the lower value. The streamlines show similar pattern with Experiment 2. Interestingly, the maximum vertical velocity peaks at 75 cm yr^{-1}, near the upper boundary of the sphere (Fig. 6a, black dashed line). This is due to the formation of a low viscosity region above the rising sphere (Fig. 5a, Experiment 4a). This experiment gives a dynamic topography of ~149 m (Fig. 6b, black dashed line). It confirms that a strong contrast in viscosity between the lithosphere and asthenosphere enhances the dynamic topography signal. We note that the viscosity contrast is attained by smoother transition between the lithosphere and asthenosphere (Fig. 7a, black dashed line). We infer the mechanical thickness of the lithosphere from the viscosity profiles plotted in Figure 7a, along which the lithosphere-asthenosphere transition zone shows a rapid decrease in viscosity (Conrad and Molnar, 1997). We observe that the effective mechanical thickness of the lithosphere is reduced to 140 km, compared to the thickness of the thermal lithosphere (Fig. 7c).

When we increase the activation volume to 27x10^{-6} m^3 mol^{-1}, the convection cells grow much larger and show continuity through the lithosphere (Fig. 5a, Experiment 4b). The sphere has a very low rising speed of ~0.25 cm yr^{-1} (Fig. 6a, black solid line). Compared to Experiment 4a, the dynamic topography shows a strong decrease from ~149 m to ~105 m (Fig. 6b, black solid line). This is an example where the system behaves nearly as a single layer with homogenous viscosity. The near absence of viscosity contrast between the lithosphere and asthenosphere explains the smaller magnitude of the dynamic topography. Moreover, the formation of moderately low viscosity channel (Fig. 7a, black solid line) also contributes to the decrease of the dynamic topography.

Deleted: of

Deleted:) in the mantle.

Deleted: asthenosphere

Deleted: This also effectively reduces

Deleted: below

Deleted: which is 150 km thick by

Deleted: definition

3.3 Numerical results: the case of wet olivine

In Experiments 5a and 5b, we consider dislocation creep of wet olivine. The reported activation volume varies between 11×10^{-6} m^3 mol^{-1} and 33×10^{-6} m^3 mol^{-1} (Hirth and Kohlstedt, 2003). In Experiment 5a, we test the lower value. The streamlines show a pattern similar to Experiment 4a, but with slightly larger convective cells (Fig. 5b, Experiment 5a). The rising velocity of the anomaly exceeds 140 cm yr^{-1} (Fig. 6a, orange dashed line), promoted by the low viscosity region sitting above the rising anomaly. The dynamic topography is ~110 m (Fig. 6b, orange dashed line). This is a bit surprising given the strong contrast in viscosity (3 orders of magnitude) between the lithosphere and asthenosphere. However, Figure 7a shows that the thickness of the mechanical lithosphere is reduced by about 30 km in comparison to Experiment 4a (e.g. 10 km reduction from thermal thickness) which resulted in lower dynamic topography with similar viscosity contrast (Figure 7b,c).

In Experiment 5b, we increase the activation volume from 11×10^{-6} m^3 mol^{-1} to 33×10^{-6} m^3 mol^{-1}. The vertical velocities show significant decrease from 140 cm yr^{-1} to 0.34 cm yr^{-1} (Fig. 6a, orange solid line). This is due to an increase in viscosity above the rising sphere. Compared to Experiment 5a, the dynamic topography decreases from ~110 m to ~90 m (Fig. 6b, orange solid line). Compared to Experiment 4b, we expect the dynamic topography to be higher due to slight increase in viscosity contrast (Fig. 7a,b). However, the increase in thickness of the low viscosity channel (Fig. 7a,d) is more effective and thereby causes a greater reduction in magnitude of the dynamic topography.

In summary, experiments using nonlinear rheology generally give lower amplitudes of dynamic topography compared to experiments using isoviscous rheology (Fig. 8). When we use dry olivine rheology for the upper mantle, the dynamic topography varies between ~105 m and ~149 m, whereas under wet conditions, the dynamic topography varies between ~90 m and

Deleted: dry
Deleted: in the mantle.
Deleted: uncertainty in
Deleted: is
Deleted: pattern with
Deleted: speed
Deleted: exceed
Deleted:). This is
Deleted: sphere
Deleted: because of
Deleted: contrast in viscosity
Deleted: viscous
Deleted: to 45
Deleted: – 30
Deleted: delivered a
Deleted: of ~149 m
Deleted: same
Deleted: viscosities
Deleted: is expected

~110 m (Fig.8). These variations are due to uncertainties in the activation volume as well as fluid content in olivine rheologies.

4. Discussion and conclusion

Using coupled 3D thermo-mechanical numerical experiments, we have modelled the dynamic topography driven by a rising sphere of 1% density anomaly, having 96 km radius and emplaced at 372 km depth. In line with analytical studies (Morgan, 1965a; Molnar et al., 2015), the experiments show that dynamic topography is sensitive to viscosity contrast between the lithosphere and asthenospheric mantle, and the thickness of the lithosphere (Fig. 7). Higher viscosity contrasts amplify the dynamic topography (Fig. 7a,b), whereas formation of a low viscosity channel just below the lithosphere has the opposite effect (Fig. 7a,d). The experiments using nonlinear rheologies show local variations in viscosity, which contribute to the dynamic thinning of the mechanical lithosphere and causes reduction in dynamic topography. In addition, models using high-activation volume creates a low viscosity channel above the density anomaly, which contributes decreasing the dynamic topography. Using a larger viscosity range in the models ($10^{18} Pa \cdot s \leq \eta(P,T,\dot{\varepsilon}) \leq 10^{23}\ Pa \cdot s$) resulted in ~5% variation in the amplitude of dynamic topography, indicating that the effects of non-linear rheology are reasonably captured in our models with smaller viscosity range ($10^{19} Pa \cdot s \leq \eta(P,T,\dot{\varepsilon}) \leq 10^{22}\ Pa \cdot s$).

Predictions of dynamic topography derived from mantle convection models are compared against residual topography which is the component of Earth's topography that is not compensated by isostasy (Flament et al., 2013; Hoggard et al., 2016). In a recent work (Cowie and Kusznir, 2018), it has been argued that dynamic topography predictions require scaling of amplitudes by ~0.75 to match the residual topography, and when density anomalies shallower than 220 km are included, the misfit requires a scaling factor of ~0.35. It is also

Deleted: By
Deleted: model
Deleted: above the rising anomaly
Deleted: result in amplification of
Deleted: reduces
Deleted: dynamic topography
Deleted: crustal
Deleted: with
Deleted: . When density anomalies are
Deleted: increases demanding

important to consider that this misfit depends on the flow wavelength and is suggested to be highest at lowest spherical harmonic degrees (2) or very long wavelengths (Steinberger, 2016). Our numerical experiments show that amplitude of dynamic topography can be nearly halved (e.g. from ~174 m in Exp. 2 to ~90 m in Exp. 5b) when we consider non-linear mantle rheology. Therefore, we propose that, at shorter wavelengths (i.e. less than 1,000 km), part of the misfit between the dynamic topography extracted from mantle convection models and dynamic topography estimated from residual topography can be attributed to the Newtonian mantle viscosity used in convection models. If the density sources are shallower, the dynamic topography becomes more sensitive to the viscosity and density structure (Morgan, 1965a; Hager and Clayton, 1989; Osei Tutu et al., 2018), and Newtonian viscosity may lead to higher misfits.

Our models suggest that for shallow density anomalies in the mantle, non-linear rheologies not only produce lateral variations in viscosity (Richards and Hager, 1989; Moucha et al., 2007), but also additional vertical variations in viscosity that impacts a relatively large area compared to the size of the anomaly in the mantle. We show that this impacts on the thickness of the mechanical lithosphere, and predictions of the amplitude of dynamic topography.

As shown in Figure 8, uncertainties on the activation volume result in variation in dynamic topography which are higher in experiments using dry olivine rheology (i.e. 17%) compared to experiments using wet olivine rheology (10%). The comparison between numerical experiments using dry olivine (Exp. 4a) and wet olivine (Exp. 5b) indicates that the variation in dynamic topography can be as much as 25%. These variations can be lessened if we have better constraints on the mantle rheology, which will advance the dynamic topography models as well as our understanding of the interaction between deep mantle and the Earth's surface.

Deleted: numerical modelling of

Deleted: explained by

Deleted: oversimplification of

Deleted: Moreover,

Deleted: as has already been shown by and

Deleted: % from an average of ~127 m)

Deleted: % from an average of ~100 m).

Deleted: % from an average of ~120 m.

Figures and Captions

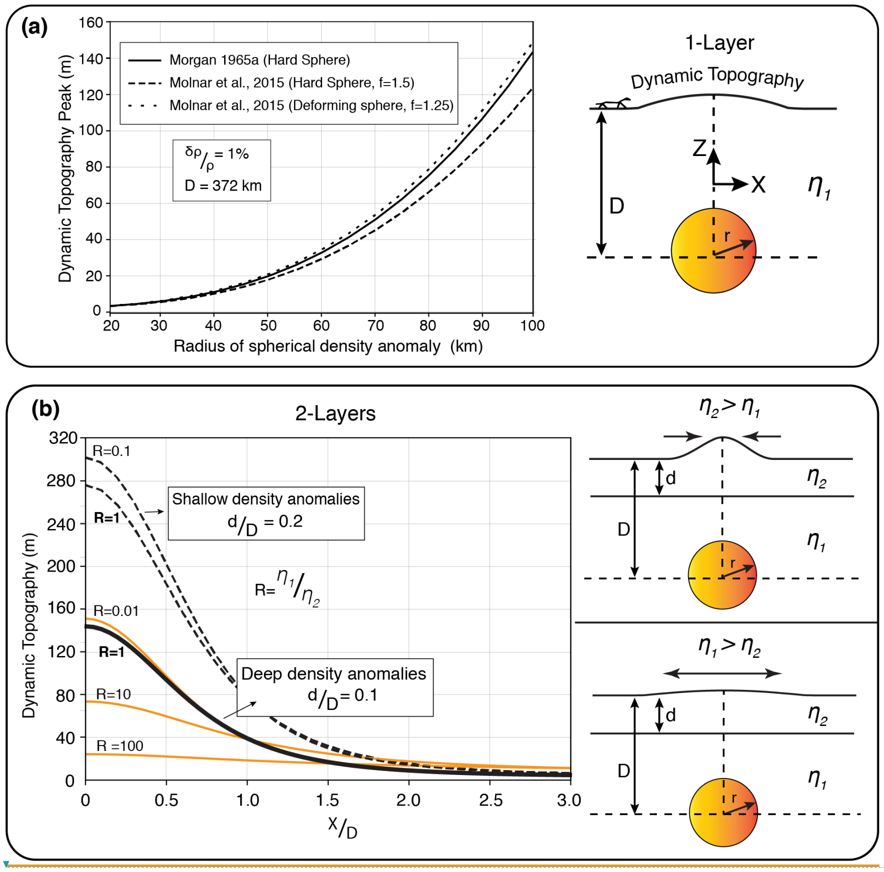

Deleted:

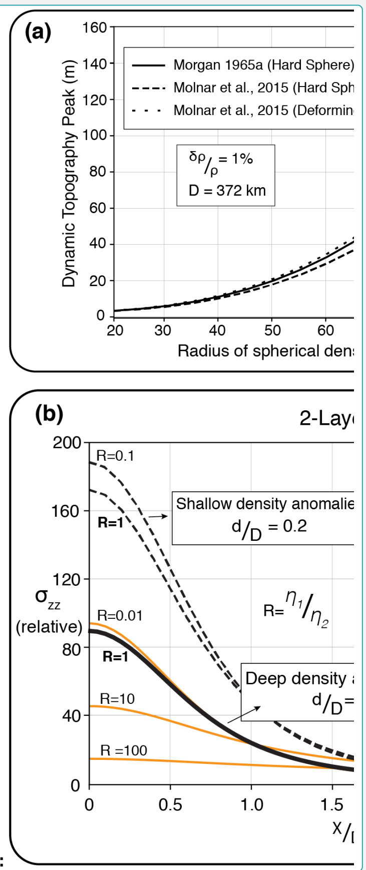

Figure 1. Dynamic topography driven by a spherical density anomaly of radius *r* at depth *D* embedded in a fluid whose viscosity structure is varied. (a) Variation in dynamic topography by radius of a spherical 1% density anomaly centred at 372 km depth in a single isoviscous fluid whose viscosity is η_1. The normal total stresses are calculated by Equation 1 taken from Morgan (1965a) (hard sphere), and Equation 3 taken from Molnar et al (2015) (hard and deforming spheres), and converted to dynamic topography by using

Deleted: in the text

Deleted: in the text

Equation 2. (b) The case where the fluid is no longer a single layer, but is composed of two layers with viscosities η_1 and η_2 for the lower and upper layers, respectively. We plot the dynamic topography for the same density anomaly in (a) using Equation 4, taken from Morgan (1965a), but with varying relative viscosities ($R=\eta_1/\eta_2$). The ratio of upper layer thickness to depth to the centre of the anomaly (d/D) also affects the dynamic topography, and higher values correspond to shallow density anomalies or thicker lithosphere for constant depth (D).

Deleted: variation in relative normal total stress at

Deleted: surface in half-space due to a spherical

Deleted: at a depth *D* with radius *r* by

Deleted: in the text

Deleted:). The plots show relative variation in stress at a relative distance of *X/D*, for different viscosity ratio of the layers

Deleted:), as well as

Deleted: of which

Deleted: more

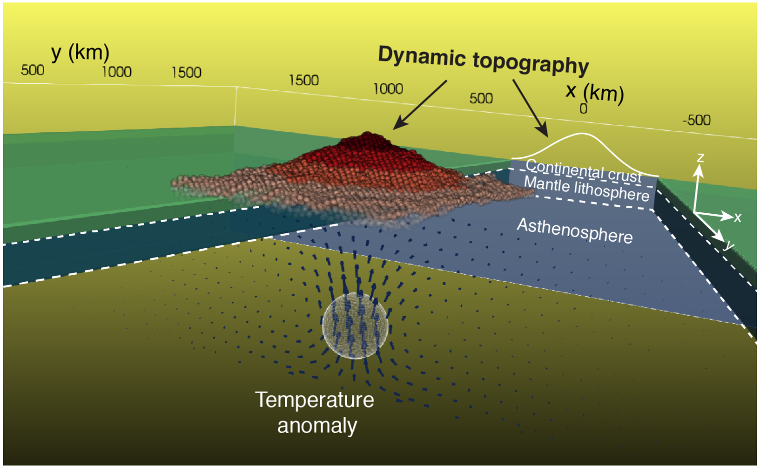

Figure 2. 3D Numerical model of a spherical temperature anomaly having 96 km radius and a density of 1% less dense than the ambient mantle embedded in a depth of 372 km. The model space is 3,840 km long in *x* and *y* axes, and 576 km deep along the *z* axis. The dynamic topography is depicted as an exaggerated surface on the top of the model and is also reflected on the *x*-*z* plane.

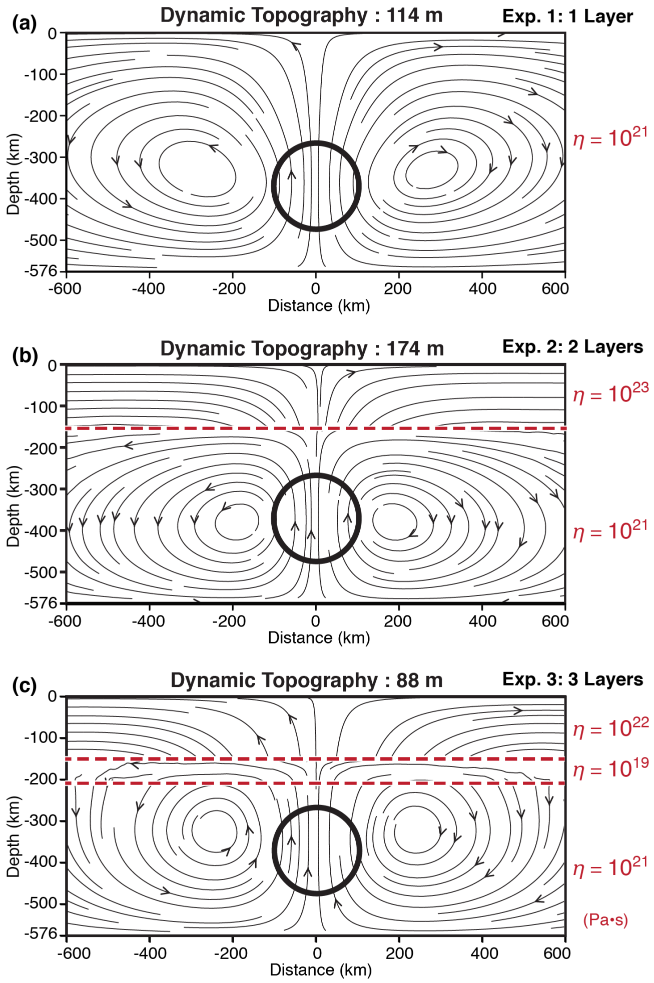

Figure 3. Predicted peak amplitudes of dynamic topography for layered Earth models with isoviscous rheology. Centred at 372 km depth, the embedded spherical density anomaly (black circle) is 96 km in radius. It has a temperature anomaly of +324 °C giving 1% effective density difference with the background. The resulting streamlines are shown in a 2D cross section (x-z plane) along the centre of each numerical model (y=0 km).

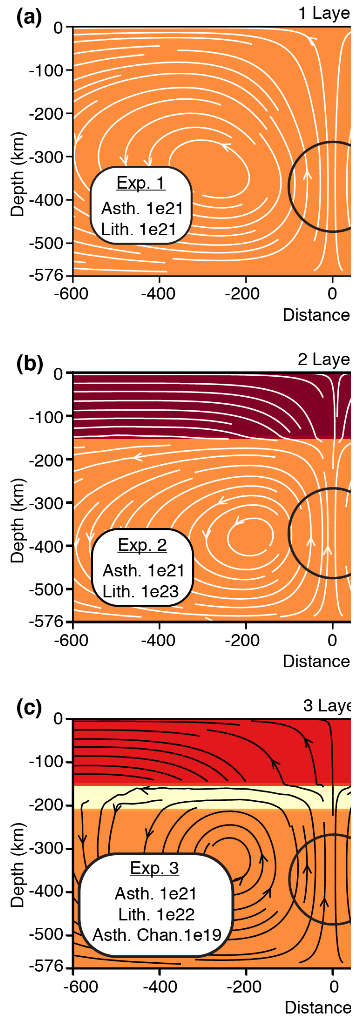

Deleted:

Deleted: Viscosity map and streamlines in a 2D cross section (x-z plane) along the centre of the numerical

Deleted: (y=0 km). All experiments include an embedded sphere

Deleted: 96 km radius and

Deleted: below the surface. The sphere (i.e.

Deleted: circles)

Deleted: (+

Deleted:)

Deleted: mantle. The ambient fluid has 1,2 or 3 isoviscous layers for Experiments 1,2 and 3 respectively.

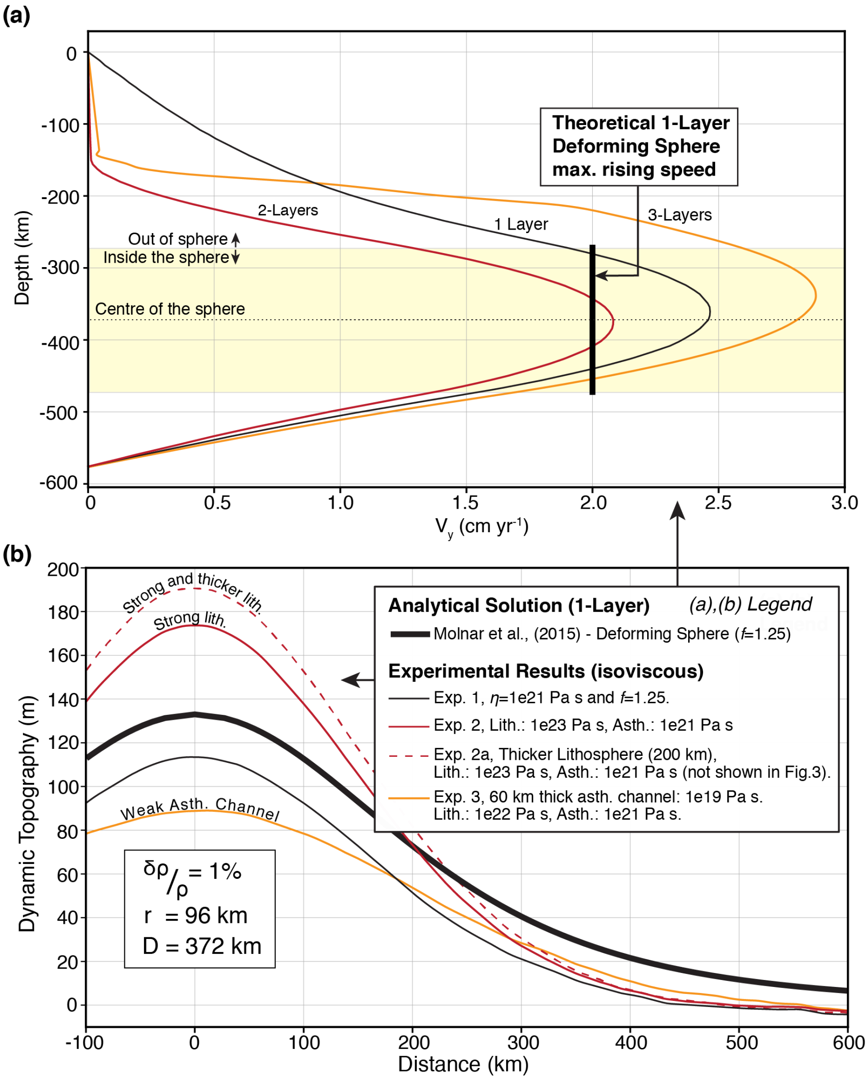

Figure 4. (a) Vertical velocity profiles (V_y) along the centre, and (b) analytical solution and numerical modelling results showing dynamic topography induced by a sphere of temperature anomaly in the mantle (r=96 km, $\delta\rho/\rho$ = 1%). The misfit between the numerical model for R=1 and the analytical solution is due to finite space in the numerical

model compared to semi-infinite space assumed in the analytical solution (Morgan 1965a).

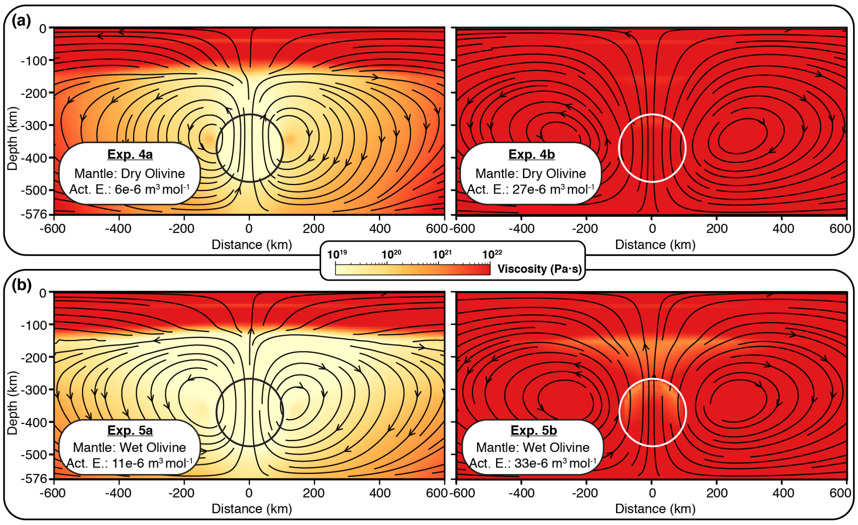

Figure 5. Viscosity map and streamlines for experiments using nonlinear rheologies (dry or wet olivine) with various activation energies. The rising sphere is shown by black or circles.

Deleted: in a 2D cross section along the centre of the numerical model (*y*=0)

Deleted: for the crust and mantle.

Deleted: with

Deleted: in each plot. In Experiments 4 and 5, the crust and mantle has visco-plastic rheologies (see Table 1 for all parameters). The crust has dislocation creep of quartzite rheology for Experiments 4a-b and Experiments 5a-b. In the mantle, the dislocation creep of dry and wet olivine rheologies are used for Experiments 4a-b and Experiments 5a-b, respectively . For each experimental set (e.g. Experiments 4a-b), we use lowest and highest activation volumes reported for the dry or wet olivine rheology .

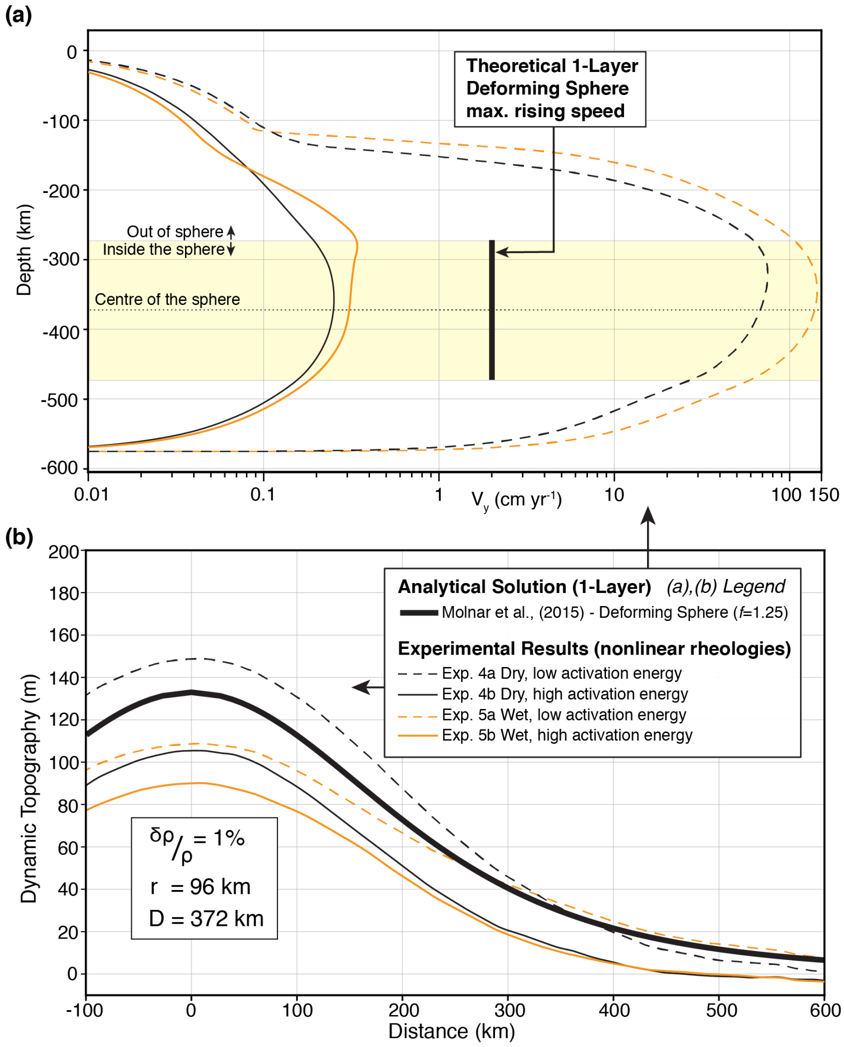

Figure 6. (a) Vertical velocity profiles (V_y) along the centre and (b) dynamic topography induced by a sphere of temperature anomaly (r=96 km, $\delta\rho/\rho$ = 1%) in the mantle that has nonlinear rheology depending on temperature, pressure and strain rate.

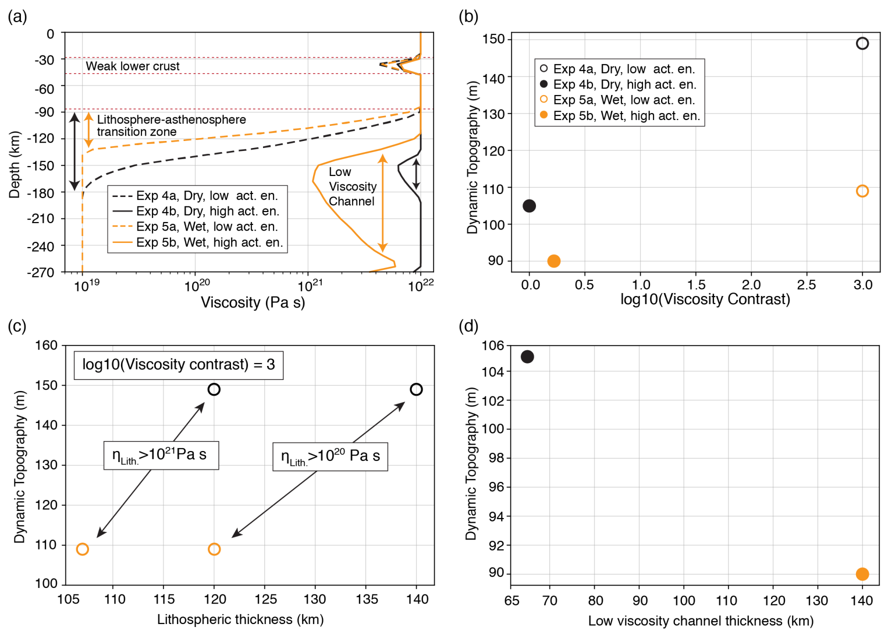

Figure 7. Factors affecting the dynamic topography. (a) Vertical viscosity profiles at the centre of the models. Variation in dynamic topography (b) by viscosity contrast between the lithosphere and part of the asthenosphere above the anomaly, (c) by lithospheric thickness (d) and by thickness of low viscosity channel.

Deleted: Important

Deleted: amplitude of

Deleted: in Experiments 4a-b and 5a-b which have nonlinear rheologies for the crust and mantle

Deleted: spherical temperature

Deleted: at constant viscosity contrast of 3 order of magnitude assuming that lithosphere-asthenosphere boundary is at 10^{20} Pa s or 10^{21} Pa s in Experiments 4a and 5a,

Deleted: above the spherical anomaly and beneath the lithosphere. This low viscosity channel forms only in Experiments 4b and 5b. In Experiments 4a and 5a, the viscosity profiles show progressive variation between the lithosphere and part of the asthenosphere above the spherical anomaly.

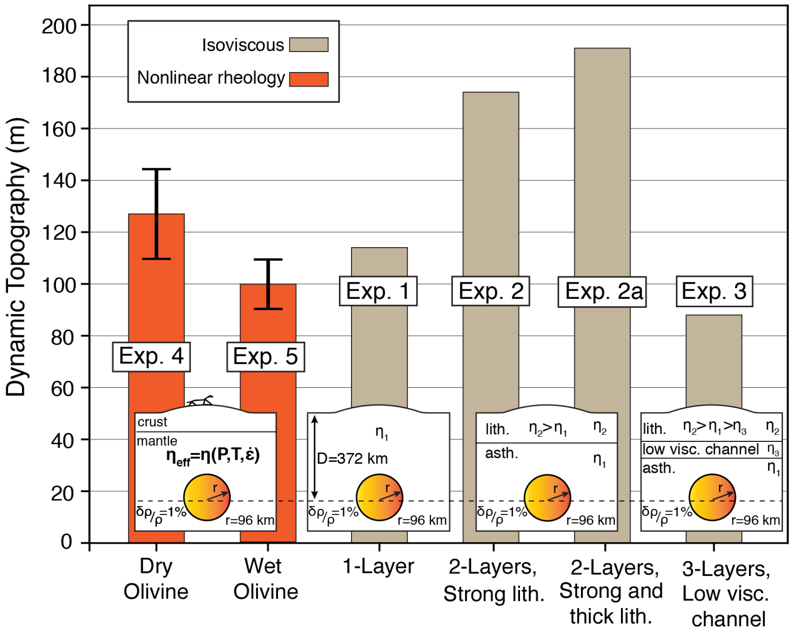

Figure 8. Predicted dynamic topographies driven by a rising sphere centred at 372 km depth with 96 km radius and 1% less dense than the ambient mantle. The various experiments differ by rheology (isoviscous vs. nonlinear) and viscous structure. For Experiments 4 and 5, we show variation in dynamic topography due to contrasting activation energy. In general, experiments with nonlinear rheologies having up to 3 orders of magnitude variation in viscosity generally predict lesser magnitude of dynamic topography compared to experiments using isoviscous rheology. Compared to dry olivine, wet olivine rheology results in lower dynamic topography.

Deleted: Compilation of

Deleted: denser from

Deleted: difference between the

Deleted: is either due to viscosity structure

Deleted: in the crust

Deleted: mantle or thickness of the lithosphere. We also show the model configurations for each experiment.

Deleted: from the average of experimental results for each experimental set (e.g. Experiments 4a-b) by using error bars. These variations correspond to experiments using different

Deleted: volumes reported for dislocation creep of dry and wet olivine rheologies .

Deleted: in the upper mantle (between 10^{19} Pa s and 10^{22} Pa s)

Deleted: Among the experiments using nonlinear rheologies, Experiment 5 which has

Deleted: the mantle gives lesser amplitude of

Deleted: compared to Experiment 4 which has dry olivine for the same material

Parameter	Symbol	EXP 4a-b,5a-b Crust[1]	EXP 4a,4b Mantle[2]	EXP 5a,5b Mantle[2]
Pre-exponential factor (MPa^{-n} s^{-1})	A	6.7×10^{-6}	1.1×10^{5}	1600
Activation energy ($kJ\ mol^{-1}$)	Q	156	530	520
Power-law exponent	n	2.4	3.5	3.5
Water fugacity	f	N.A.	N.A.	1000
Water fugacity exponent	r	N.A.	N.A.	1.2
Activation volume ($m^3\ mol^{-1}$)	V	0.0	6×10^{-6} or 27×10^{-6}	11×10^{-6} or 33×10^{-6}
Reference density ($kg\ m^{-3}$)	ρ_0	2,700	3,370	3,370
Reference temperature (K)	T	293.15	293.15	293.15
Initial cohesion (MPa)	C_0	10	10	10
Cohesion after weakening (MPa)	C_1	2	2	2
Initial coefficient of friction	μ_0	0.577	0.577	0.577
Coefficient of friction after weakening	μ_1	0.017	0.017	0.017
Saturation strain	ϵ_{max}	0.2	0.2	0.2
Thermal diffusivity ($m^2\ s^{-1}$)	κ	1×10^{-6}	1×10^{-6}	1×10^{-6}
Thermal expansivity (K^{-1})	α	3×10^{-5}	3×10^{-5}	3×10^{-5}
Compressibility (MPa^{-1})	β	4×10^{-5}	0	0
Heat capacity ($J\ K^{-1}\ kg^{-1}$)	C_P	1,000	1,000	1,000
Radiogenic heat production ($W\ m^{-3}$)	H	0.5×10^{-6}	0.2×10^{-7}	0.2×10^{-7}

Table 1. Thermal and rheological parameters. We use the rheological parameters from (1) quartzite (Ranalli, 1995), (2) dry or wet olivine (Hirth and Kohlstedt, 2003).

Author contribution

Ö.F.B designed the experiments and wrote the manuscript. P.F.R. contributed to the analysis of numerical modelling results and improved the manuscript.

Inserted Cells
Deleted: Parameters
Deleted: Mantle[3]
Deleted: Grain size exponent ... [1]
Inserted Cells
Deleted: expans.
Deleted: for all experiments. References we are based on using
Deleted: are
Deleted: dislocation creep of dry olivine and (3) dislocation creep of
Deleted: Activation volume is varied in experimental sets of 4a-b, and 5a-b.
Deleted: improved the manuscript and
Deleted: in discussion

Competing interests

The authors declare that they have no conflict of interest.

Code and data availability

In our experiments, we used Underworld, a free open-source code developed under the Australian Auscope initiative.

The version of *Underworld* code we used in our study can be found at:

https://github.com/OlympusMonds/EarthByte_Underworld

To follow an open-source philosophy and promote reproducible science, our input scripts (a suite of xml input scripts) will be available directly through the EarthByte's freely accessible web server as well as author's GitHub repository.

Acknowledgements

This research was undertaken with the assistance of resources from the National Computational Infrastructure (NCI), through the National Computational Merit Allocation Scheme supported by the Australian Government; the Pawsey Supercomputing Centre with funding from the Australian Government and the Government of Western Australia, and support from the Australian Research Council through the Industrial Transformation Research Hub grant ARC-IH130200012.

References

Becker, T. W.: Superweak asthenosphere in light of upper mantle seismic anisotropy, Geochemistry, Geophys. Geosystems, 18(5), 1986–2003, doi:10.1002/2017GC006886, 2017.

Braun, J.: The many surface expressions of mantle dynamics, Nat. Geosci., 3(12), 825–833, doi:10.1038/ngeo1020, 2010.

Cammarano, F., Goes, S., Vacher, P. and Giardini, D.: Inferring upper-mantle temperatures from seismic velocities, Phys. Earth Planet. Inter., 138(3–4), 197–222, doi:10.1016/S0031-9201(03)00156-0, 2003.

Cazenave, A., Souriau, A. and Dominh, K.: Global coupling of Earth surface topography with hotspots, geoid and mantle heterogeneities, Nature, 340(6228), 54–57, doi:10.1038/340054a0, 1989.

Chopra, P. N. and Paterson, M. S.: The role of water in the deformation of dunite, , 89(B9), 7861–7876, 1984.

Conrad, C. P. and Husson, L.: Influence of dynamic topography on sea level and its rate of changeInfluence of dynamic topography on sea level, Lithosphere, 1(2), 110–120, doi:10.1130/L32.1, 2009.

Conrad, C. P. and Molnar, P.: The growth of Rayleigh-Taylor-type instabilities in the lithosphere for various rheological and density structures, , 95–112, 1997.

Cowie, L. and Kusznir, N.: Renormalisation of global mantle dynamic topography predictions using residual topography measurements for “normal” oceanic crust, Earth Planet. Sci. Lett., 499, 145–156, doi:10.1016/j.epsl.2018.07.018, 2018.

Craig, C. H. and McKenzie, D.: The existence of a thin low-viscosity layer beneath the lithosphere, Earth Planet. Sci. Lett., 78(4), 420–426, 1986.

Crough, S. T.: Hotspot swells, Annu. Rev. Earth Planet. Sci., 11(1), 165–193, 1983.

Davies, D. R., Valentine, A. P., Kramer, S. C., Rawlinson, N., Hoggard, M. J., Eakin, C. M. and Wilson, C. R.: Earth’s multi-scale topographic response to global mantle flow, Nat. Geosci., 12, 845–850, 2019.

Davies, G. F. and Pribac, F.: Mesozoic seafloor subsidence and the Darwin Rise, past and present, Washingt. DC Am. Geophys. Union Geophys. Monogr. Ser., 77, 39–52, 1993.

Flament, N., Gurnis, M. and Müller, R. D.: A review of observations and models of dynamic topography, Lithosphere, 5(2), 189–210, doi:10.1130/L245.1, 2013.

Forte, A. M. and Mitrovica, J. X.: New inferences of mantle viscosity from joint inversion of long-wavelength mantle convection and post-glacial rebound data, Geophys. Res. Lett., 23(10), 1147–1150, doi:10.1029/96GL00964, 1996.

Gleason, G. C. and Tullis, J.: A flow law for dislocation creep of quartz aggregates determined with the molten salt cell, Tectonophysics, 247(1–4), 1–23, doi:10.1016/0040-1951(95)00011-B, 1995.

Griffiths, R. W., Gurnis, M. and Eitelberg, G.: Holographic measurements of surface topography in laboratory models of mantle hotspots, Geophys. J. Int., 96(3), 477–495, 1989.

Gurnis, M., Mitrovica, J. X., Ritsema, J. and Van Heijst, H. J.: Constraining mantle density structure using geological evidence of surface uplift rates: The case of the African Superplume, Geochemistry, Geophys. Geosystems, 1(7), doi:10.1029/1999GC000035, 2000.

Hager, B. H.: Constraints on Mantle Rheology and Flow, J. Geophys. Res., 89(B7), 6003–6015, 1984.

Hager, B. H. and Clayton, R. W.: Constraints on the structure of mantle convection using seismic observations, flow models, and the geoid, 1989.

Hager, B. H., Clayton, R. W., Richards, M. A., Comer, R. P. and Dziewonski, A. M.: Lower mantle heterogeneity, dynamic topography and the geoid, Nature, 313(6003), 541, 1985.

Hirth, G. and Kohlstedt, D.: Rheology of the upper mantle and the mantle wedge: A view from the experimentalists, Insid. subduction Fact., 138, 83–105, 2003.

Hoggard, M. J., White, N. and Al-Attar, D.: Global dynamic topography observations reveal limited influence of large-scale mantle flow, Nat. Geosci., 9(6), 456–463, doi:10.1038/ngeo2709, 2016.

Houseman, G. A. and Hegarty, K. A.: Did rifting on Australia's Southern Margin result from tectonic uplift?, Tectonics, 6(4), 515–527, doi:10.1029/TC006i004p00515, 1987.

Isacks, B., Oliver, J. and Sykes, L. R.: Seismology and the new global tectonics, J. Geophys. Res., 73(18), 5855–5899, 1968.

Karato, S.: On the Lehmann discontinuity, Geophys. Res. Lett., 19(22), 2255–2258, 1992.

Karato, S. and Wu, P.: Rheology of the upper mantle: a synthesis., Science, 260(5109), 771–778, doi:10.1126/science.260.5109.771, 1993.

Kaufmann, G. and Lambeck, K.: Mantle dynamics, postglacial rebound and the radial viscosity profile, Phys. Earth Planet. Inter., 121(3–4), 301–324, doi:10.1016/S0031-9201(00)00174-6, 2000.

Korenaga, J. and Karato, S.: A new analysis of experimental data on olivine rheology, J. Geophys. Res. Solid Earth, 113(B2), 2008.

Mitrovica, J. X. and Forte, A. M.: Radial profile of mantle viscosity: Results from the joint inversion of convection and postglacial rebound observables, J. Geophys. Res., 102(B2), 2751, doi:10.1029/96JB03175, 1997.

Molnar, P. and Tapponnier, P.: Cenozoic tectonics of Asia: effects of a continental collision, Science (80-.)., 189(4201), 419–426, 1975.

Molnar, P., England, P. C. and Jones, C. H.: Mantle dynamics, isostasy, and the support of high terrain, J. Geophys. Res. Solid Earth, 1–26, doi:10.1002/2014JB011724, 2015.

Moresi, L., Dufour, F. and Mühlhaus, H.-B.: A Lagrangian integration point finite element method for large deformation modeling of viscoelastic geomaterials, J. Comput. Phys., 184(2), 476–497, doi:10.1016/S0021-9991(02)00031-1, 2003.

Moresi, L., Quenette, S., Lemiale, V., Mériaux, C., Appelbe, B. and Mühlhaus, H.-B.: Computational approaches to studying non-linear dynamics of the crust and mantle, Phys. Earth Planet. Inter., 163(1–4), 69–82, doi:10.1016/j.pepi.2007.06.009, 2007.

Morgan, W. J.: Gravity anomalies and convection currents: 1. A sphere and cylinder sinking

beneath the surface of a viscous fluid, J. Geophys. Res., 70(24), 6175–6187, 1965a.
Morgan, W. J.: Gravity anomalies and convection currents: 2. The Puerto Rico Trench and the Mid-Atlantic Rise, J. Geophys. Res., 70(24), 6189–6204, 1965b.
Moucha, R. and Forte, A. M.: Changes in African topography driven by mantle convection, Nat. Geosci., 4, 707 [online] Available from: https://doi.org/10.1038/ngeo1235, 2011.
Moucha, R., Forte, A. M., Mitrovica, J. X. and Daradich, A.: Lateral variations in mantle rheology: Implications for convection related surface observables and inferred viscosity models, Geophys. J. Int., 169(1), 113–135, doi:10.1111/j.1365-246X.2006.03225.x, 2007.
Moucha, R., Forte, A. M., Mitrovica, J. X., Rowley, D. B., Quéré, S., Simmons, N. A. and Grand, S. P.: Dynamic topography and long-term sea-level variations: There is no such thing as a stable continental platform, Earth Planet. Sci. Lett., 271(1–4), 101–108, 2008.
Osei Tutu, A., Steinberger, B., Sobolev, S. V, Rogozhina, I. and Popov, A. A.: Effects of upper mantle heterogeneities on the lithospheric stress field and dynamic topography, Solid Earth, 9(3), 649–668, 2018.
Parsons, B. and Daly, S.: The relationship between surface topography, gravity anomalies and temperature structure of convection., J. Geophys. Res., 88(B2), 1129–1144, doi:10.1029/JB088iB02p01129, 1983.
Pekeris, C. L.: Thermal convection in the interior of the Earth., Geophys. Suppl. Mon. Not. R. Astron. Soc., 3, 343–367, 1935.
Phipps Morgan, J., Morgan, W. J., Zhang, Y.-S. and Smith, W. H. F.: Observational hints for a plume-fed, suboceanic asthenosphere and its role in mantle convection, J. Geophys. Res. Solid Earth, 100(B7), 12753–12767, doi:10.1029/95JB00041, 1995.
Post, R. L. and Griggs, D. T.: The earth's mantle: evidence of non-Newtonian flow, Science (80-.)., 181(4106), 1242–1244, 1973.
Ranalli, G.: Rheology of the Earth, 2nd ed., Chapman & Hall, London., 1995.

Richards, M. A. and Hager, B. H.: Effects of lateral viscosity variations on long-wavelength geoid anomalies and topography, J. Geophys. Res. Solid Earth, 94(B8), 10299–10313, 1989.

Sembroni, A., Kiraly, A., Faccenna, C., Funiciello, F., Becker, T. W., Globig, J. and Fernandez, M.: Impact of the lithosphere on dynamic topography: Insights from analogue modeling, Geophys. Res. Lett., 44(6), 2693–2702, doi:10.1002/2017GL072668, 2017.

Steinberger, B.: Effects of latent heat release at phase boundaries on flow in the Earth's mantle, phase boundary topography and dynamic topography at the Earth's surface, Phys. Earth Planet. Inter., 164(1–2), 2–20, 2007.

Steinberger, B.: Topography caused by mantle density variations: observation-based estimates and models derived from tomography and lithosphere thickness, Geophys. Suppl. to Mon. Not. R. Astron. Soc., 205(1), 604–621, 2016.

Steinberger, B., Conrad, C. P., Osei Tutu, A. and Hoggard, M. J.: On the amplitude of dynamic topography at spherical harmonic degree two, Tectonophysics, 760(November 2017), 221–228, doi:10.1016/j.tecto.2017.11.032, 2019.

Stern, R. J.: Subduction zones, Rev. Geophys., 40(December), 1031–1039, doi:10.1029/2001RG000108, 2002.

Stixrude, L. and Lithgow-Bertelloni, C.: Mineralogy and elasticity of the oceanic upper mantle: Origin of the low-velocity zone, J. Geophys. Res. Solid Earth, 110(3), 1–16, doi:10.1029/2004JB002965, 2005.

Page 24: [1] Deleted	Omer Bodur	14/11/2019 11:27:00

Grain size exponent	0.0	0.0	0.0